Journal of Applied Physics

Intersubband transitions in nonpolar and semipolar III-nitrides: Materials, devices, and applications

Cite as: J. Appl. Phys. **131**, 210901 (2022); https://doi.org/10.1063/5.0088021
Submitted: 11 February 2022 • Accepted: 11 May 2022 • Published Online: 02 June 2022

Dinusha Herath Mudiyanselage, Dawei Wang, Yuji Zhao, et al.

Journal of Applied Physics PERSPECTIVE scitation.org/journal/jap

Intersubband transitions in nonpolar and semipolar III-nitrides: Materials, devices, and applications

Cite as: J. Appl. Phys. **131**, 210901 (2022); doi: 10.1063/5.0088021
Submitted: 11 February 2022 · Accepted: 11 May 2022 ·
Published Online: 2 June 2022

Dinusha Herath Mudiyanselage,[1] Dawei Wang,[1] Yuji Zhao,[2] and Houqiang Fu[1,a)]

AFFILIATIONS

[1]Department of Electrical and Computer Engineering, Iowa State University, Ames, Iowa 50011, USA
[2]Department of Electrical and Computer Engineering, Rice University, Houston, Texas 77005, USA

[a)]**Author to whom correspondence should be addressed:** houqiang@iastate.edu

ABSTRACT

In the last two decades, the third-generation wide bandgap semiconductor III-nitrides have revolutionized a myriad of electronic and photonic devices and applications, including power electronics, extreme-environment electronics, RF amplifiers, and optoelectronics such as light-emitting diodes and laser diodes. Recently, III-nitride heterostructures (e.g., AlGaN/GaN) based intersubband transition (ISBT) has garnered considerable research interest for infrared (IR), terahertz (THz), and ultrafast optoelectronics (e.g., photodetectors and quantum cascade lasers) due to its large conduction band offset, large optical phonon energy, and promising room-temperature operation. This paper presents a comprehensive review on the recent progress and challenges of III-nitrides based ISBT from the perspectives of materials, structures, devices, and applications, with a focus on nonpolar and semipolar III-nitrides. Various device structures have been demonstrated for III-nitrides based ISBT, including quantum wells, dots, and wires, among which AlGaN/GaN quantum wells are the most widely used. The effects of device parameters, crystal orientations, and doping on the ISBT properties of AlGaN/GaN quantum wells are discussed. Although the room-temperature operation is still elusive, theoretical and experimental studies show that nonpolar and semipolar III-nitrides based ISBT exhibits tunable ISBT wavelength from far-IR to THz spectral range with higher efficiency compared with polar *c*-plane ISBT. This review can serve as a gateway to and an important reference for the recent progress and challenges of III-nitrides based ISBT and its potential applications in sensing, communication, ultrafast optoelectronics, and integrated photonics.

I. INTRODUCTION

III-nitrides have attracted tremendous research interest for power electronics,[1,2] RF electronics,[3] light-emitting diodes (LEDs), and laser diodes (LDs).[4–7] Moreover, due to large conduction band offsets and optical phonon energy, III-nitrides based heterostructures (e.g., AlGaN/GaN) have enabled intersubband transition (ISBT) based optoelectronic devices such as quantum well infrared photodetectors (QWIPs),[8–10] terahertz (THz) intersubband (ISB) photodetectors,[9] quantum cascade detectors (QCDs),[9–12] quantum cascade lasers (QCLs),[9,13] resonant tunneling diodes (RTDs), electro-optical modulators, and all-optical switches.[9–11] In a quantum well (QW) structure, ISBT refers to the optical transition between sub-bands in the conduction band, while the transition between valance and conduction bands is interband (IB) transitions. Epitaxial growth techniques that can control atomic-layer thickness, such as molecular beam epitaxy (MBE) and metalorganic chemical vapor deposition (MOCVD), have made the growth of ISBT devices possible.[10] Although the first ISBT was observed in two-dimensional electron gas (2DEG)[14] at semiconductor heterojunctions, the QW ISBT was first reported in the AlGaAs/GaAs system in 1985.[15] Suzuki and Iizuka[16] theoretically predicted the ISBT in AlGaN/GaN QW, which was experimentally demonstrated in 1997.[17] Soon after this progress, the potential of III-nitride ISBT has been widely recognized, paving the path to III-nitride ISBT based various optoelectronic devices and applications.[9–12] AlGaAs/GaAs ISBT based systems can be tuned to mid-infrared (mid-IR) to THz spectral range. However, shorter wavelengths (i.e., $<3\,\mu$m) are difficult to realize in the AlGaAs/GaAs system due to its limited conduction band offset of

~0.35 eV[10] and material transparency.[11] In contrast, III-nitrides can exhibit large conduction band offset (~1.75 eV for AlN/GaN)[18] and large longitudinal optical (LO) phonon energy (~92 meV for GaN), which could achieve excellent device performance at high temperatures in THz frequencies (1–10 THz) and near-IR wavelengths (<3 μm) with ultrafast carrier dynamics (~100 fs).[9] Furthermore, (Al)GaN is transparent for a wide spectral range (360 nm to 13 μm for GaN[11]), which makes it a more attractive candidate for ISBT devices. However, the ISBT oscillator strength is smaller in GaN than in GaAs due to other factors such as effective mass (GaN ~ $0.2m_0$[11] and GaAs ~ $0.063m_0$,[19] where m_0 is the free electron mass). In this paper, the recent progress of III-nitrides based ISBT will be comprehensively discussed in terms of ISBT materials, structures, devices, and applications. III-nitrides ISBT based on various device structures will be studied, including QWs, quantum dots (QDs), quantum wires, and cubic III-nitrides. The effects of device parameters (i.e., thickness and alloy content), polarizations, and doping on the ISBT wavelength and response of AlGaN/GaN QW will be thoroughly investigated. Theoretical and experimental nonpolar and semipolar nitride ISBT will also be discussed. It is revealed that nonpolar and semipolar III-nitrides with reduced polarizations can achieve wide tunable spectra wavelength range from IR to THz and higher efficiency, which opens the door to various ISBT based applications in sensing, biomedical imaging, communication, photonic device integration, and ultrafast optoelectronics.

II. III-NITRIDE MATERIALS FOR ISBT

III-nitrides, i.e., (In, Ga, Al)N, crystallize into the wurtzite structure, which is formed by two hexagonal close-packed sublattices. Due to the lack of inversion symmetry, III-nitrides exhibit spontaneous polarization (P_{sp}), resulting from a shift between cation and anion sub-lattices along the [0001] direction.[20] In addition, strain due to lattice mismatch in III-nitride heterostructures (e.g., AlGaN/GaN and InGaN/GaN) also results in piezoelectric polarization (P_{PZ}). The total polarization (ΔP_{tot}) of the heterostructures is the sum of spontaneous and piezoelectric polarization differences at the heterostructure interface. It should be noted that these polarization effects are crystal orientation-dependent, where the strongest polarization is along the *c*-axis or the [0001] direction, i.e., polar plane. Planes with non-zero polarization (except for the *c*-plane) are known as semipolar planes, whereas planes with zero polarization are known as nonpolar planes (*a*- and *m*-planes) [Fig. 1(a)]. The planes are also denoted by a certain inclination angle θ from the *c*-plane, and the polarization effects in III-nitrides vary with the plane's inclination angle θ [Fig. 1(b)].

The spontaneous and piezoelectric polarizations in *c*-plane III-nitrides lead to strong electric fields inside III-nitride QWs, resulting in a tilted band profile [Fig. 1(c)] and a quantum confined Stark effect (QCSE). This tilted band profile reduces the spatial wavefunction overlap in IB transitions and decreases the transition strength as the transition occurs between conduction and valence

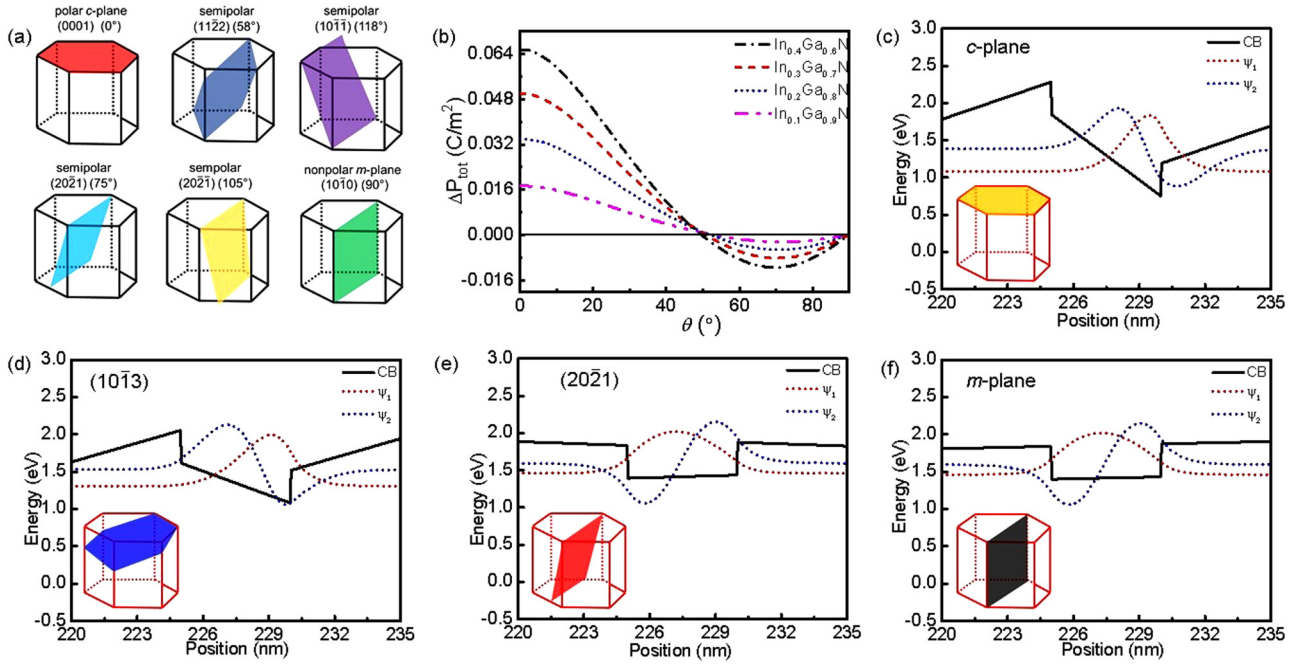

FIG. 1. (a) Schematics of polar (*c*-plane), semipolar ((11$\bar{2}$2), (10$\bar{1}$1), (20$\bar{2}$1), and (20$\bar{2}$1)), and nonpolar plane (*m*-plane) of the wurtzite crystal structure. (b) Total polarization field of $In_xGa_{1-x}N$ with the inclination angle θ (x = 0.1–0.4).[21] First two sub-bands' wavefunctions ψ_1 and ψ_2 and conduction band (CB) profile of a single QW (SQW) on (c) *c*-plane, (d) (10$\bar{1}$3) plane, (e) (20$\bar{2}$1) plane, and (f) *m*-plane.[22] (a) and (b) Reproduced with permission from Zhao *et al.*, Adv. Opt. Photonics **10**, 246 (2018). Copyright 2018 Optica Publishing Group. (c)–(f) Reproduced with permission from Fu *et al.*, J. Appl. Phys. **119**, 174502 (2016). Copyright 2016 AIP Publishing LLC.

bands. For ISBT, the tilted band profile hinders the ability to tune the energy differences between sub-bands via varying well width due to the bounded energy of the lowest states. In order to mitigate the polarization effects along the *c*-axis, nonpolar [Fig. 1(f)] and semipolar planes [Figs. 1(d) and 1(e)] with no or eliminated polarizations are proposed to enhance the ISBT in III-nitrides. Although nonpolar planes do not exhibit polarizations, material growth on nonpolar planes can be challenging due to high defect densities, strong anisotropy, cracking, hillocks, and basal plane stacking faults.[23] An alternative route is to use semipolar planes with reduced polarizations and internal electric fields and lower in-plane anisotropy. It is essential to choose low-polarization semipolar planes for the devices such as $(10\bar{1}\bar{1})$, $(20\bar{2}1)$, $(20\bar{2}\bar{1})$, and $(30\bar{3}\bar{1})$ planes.[21] In terms of theory, the polarization-induced selection rules of ISBT can be found in Refs. 9, 10, and 24. Usually, the ISB transmission or ISB absorption is measured by the polarized attenuated total reflectance (ATR)[25] with a 45° prism.

III. III-NITRIDE ISBT STRUCTURES

A. AlGaN/GaN QW

AlGaN/GaN QW structures are widely used for ISBT due to their large conduction band offset. Al content in the AlGaN barrier can impact the strain and piezoelectric polarization of the heterostructure and the ISBT wavelength. Furthermore, growing high-Al-content AlGaN is also challenging due to material degradation. After laying the theoretical foundation for AlGaN/GaN ISBT,[16,26] Suzuki and Iizuka[27] showed the absorption in the 3–4 μm range for $Al_{0.65}Ga_{0.35}N$/GaN multiple QWs (MQWs). It was found that a strong built-in polarization of ~2 MV/cm was present inside the QW, and reducing the electric field in the barriers is necessary to obtain shorter ISBT wavelengths. Iizuka *et al.*[28] reported <150 fs ISB relaxation time at 4.6 μm for $Al_{0.65}Ga_{0.35}N$/GaN MQWs. Gmachl *et al.* demonstrated that it was possible to achieve telecommunication wavelength of 1.55 μm using AlGaN/GaN heterostructures.[29–33] The lower-Al-content AlGaN layer was used to obtain better interface quality of the heterostructure and longer ISB absorption wavelengths. Péré-Laperne *et al.* reported tunable ISB absorption in the 4.5–5.3 μm using $Al_{0.2}Ga_{0.8}N$/GaN superlattices (SLs) grown by MOCVD.[34]

Kandaswamy *et al.*[35] reported mid-IR ISB absorption in AlGaN/GaN SLs on GaN-on-Si(111) templates using plasma-assisted MBE (PAMBE). The SLs consisted of 40 periods of Si-doped $Al_xGa_{1-x}N$/GaN QWs on GaN and $Al_xGa_{1-x}N$ buffer. Figure 2(a) shows the shift of ISB wavelength as a function of the Al mole fraction. With decreasing Al mole fraction, ISB wavelength increased, indicating that energy separation between two sub-bands decreased. This is attributed to a reduced conduction band offset with low Al mole fraction in the AlGaN barrier. When the Al mole fraction was lower than 0.2, the QW could not confine two sub-bands, hence no ISB absorption was observed. Figure 2(b) demonstrates the TM-polarized ISB absorption in the range of 3–9 μm with varying Al mole fraction and well/barrier thickness to cover mid-IR wavelengths.[35] With decreasing Al mole fraction, the absorption peak shifted to longer wavelengths. Spectral broadening was not due to dislocations in GaN-on-Si but caused by thickness fluctuations and alloy inhomogeneities. Furthermore, QW doping can also affect the band structure and ISB energy by the screening of polarization-induced electric field. Kandaswamy *et al.*[36] investigated the effect of doping on the mid-IR ISB absorption in AlGaN/GaN SLs grown on GaN-on-Si templates. Si doping was varied between 1×10^{19} and 5×10^{20} cm^{-3} with uniform layers and sharp interfaces [Fig. 2(c)]. ISB absorption spectra were obtained at room-temperature using Fourier transform infrared (FTIR) spectroscopy [Fig. 2(d)]. At high doping, ISB energy difference increased, ISB absorption blue-shifted, and spectra linewidth broadened due to electric field screening and band filling in the QW. It should be noted that wavelength blue-shifting can also be induced by many-body interaction of intentional or unintentional dopants in the III-nitrides QW.

AlGaN/GaN QW ISBTs are very efficient in mid-IR spectral range and can be extended to the THz regime[36] by reducing the internal electric field, such as reducing barrier Al content, increasing the well thickness, and decreasing the barrier thickness. In addition, Machandani *et al.*[37] proposed a flatband potential profile using AlGaN/GaN step QW, as shown in Fig. 2(e). The structure consisted of a GaN well, an $Al_{0.05}Ga_{0.95}N$ step barrier, and an $Al_{0.1}Ga_{0.9}N$ barrier. Due to the step barrier, the electron wave functions are spread and confined between the GaN QW and step barrier. This allows the wavefunctions to behave like a flat QW profile without polarization-induced effects. Two different samples with different step barrier lengths of 10 and 15 nm were fabricated. Measurements performed at 4.7 K using FTIR spectroscopy showed ISB absorption at 2–4 THz due to the flatband engineering of GaN ISB devices.

B. AlN/GaN QW

AlN/GaN QWs are also attractive for ISBT due to large conduction band offset of 1.75 eV, large LO phonon energy of 92 meV, and extremely short ISB absorption recovery time of 140–400 ps.[38] Kandaswamy *et al.*[38] extensively investigated AlN/GaN short-period SLs for ISB optoelectronics. Series of AlGaN/GaN MQWs width different QW widths were grown. The structures were unintentionally doped or Si-doped at different locations such as barrier, well, middle of the well, and middle of the barrier to study the effect of doping on ISBT. Figure 3(a) represents the experimental and theoretical ISBT energy ($e_1 - e_2$ and $e_1 - e_3$) with varying QW widths. The ISBT energy decreased with increasing the QW width, which is consistent with previous discussions. Figure 3(b) shows the TM-polarized absorption spectra for AlN/GaN MQWs with different cap layers. With increasing Al content in the cap layer, the absorption spectrum broadened, which can be explained by Fig. 3(c). With the AlN cap layer, the conduction band of the first GaN QW was below the Fermi level and responsible for the dominant IR absorption. In contrast, the GaN cap layer depletes the MQW active region, leading to poor IR absorption. This indicates that the cap layer can modify the internal polarization field inside QWs and impact the ISBT.

C. In-containing III-nitride QW

For Al(Ga)N/GaN QW, there is about 2.5% in-plane lattice mismatch between AlN/GaN, and increasing Al content will lead to higher defect densities and cracks. Moreover, alloy disorder and

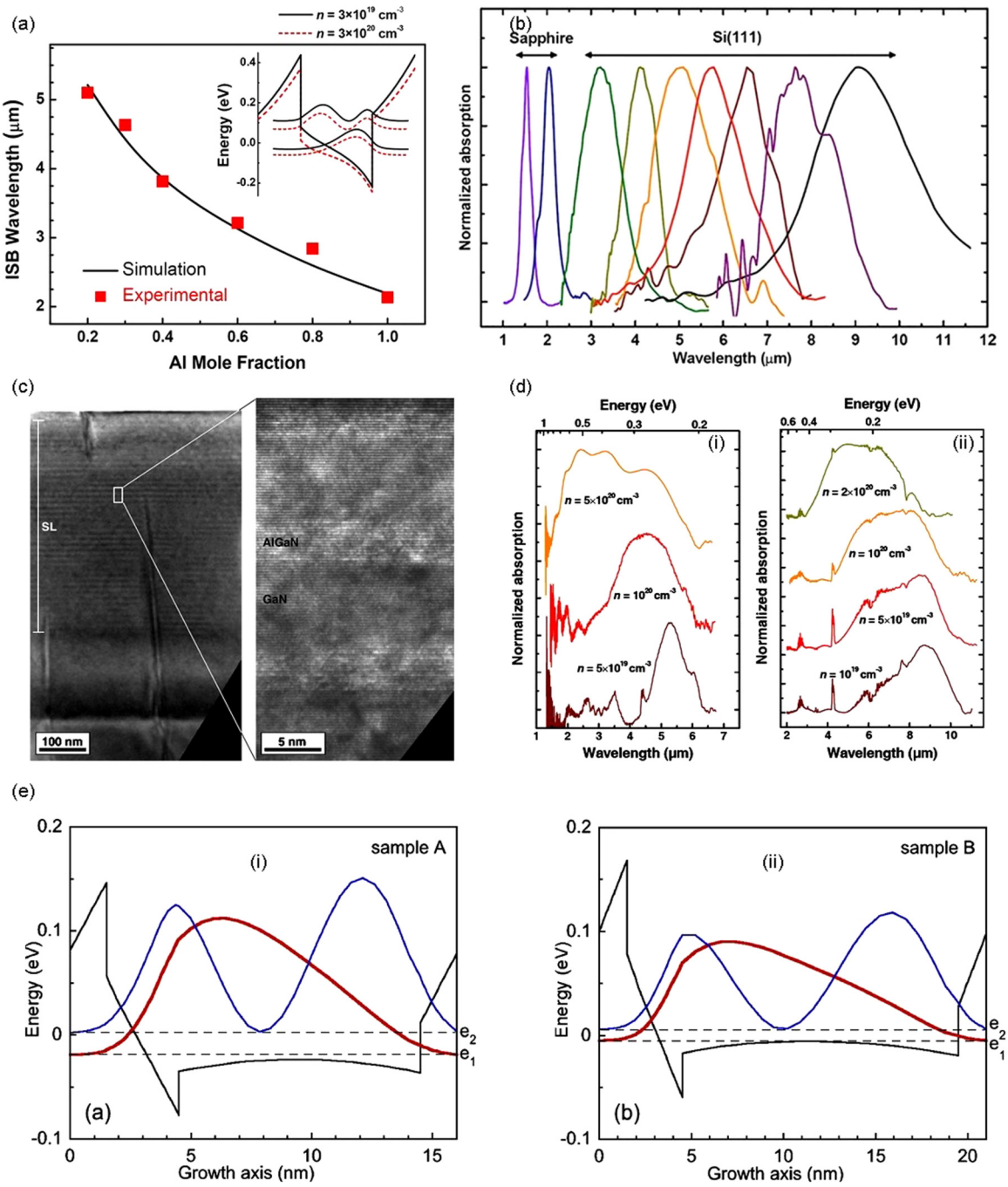

FIG. 2. (a) Theoretical and experimental variation of ISB absorption wavelength with the Al content in the barrier of AlGaN/GaN (3/3) nm superlattices (SLs). Inset: Effect of doping on the e_1 and e_2 sub-bands in a AlGaN/GaN (3/5) nm SL. (b) IR absorption spectra for TM-polarized light measured in AlGaN/GaN SLs with different barrier Al contents and QW width, grown either on sapphire or on Si(111) templates.[35] (c) Cross-sectional transmission electron microscope (TEM) image of the Si-doped $Al_{0.1}Ga_{0.9}N$/GaN (4/7) nm SL structure grown on GaN-on-Si(111) and high-resolution TEM (HR-TEM) image illustrating three periods of the SL. (d) IR absorption spectra for TM-polarized light measured from (i) $Al_{0.2}Ga_{0.8}N$/GaN (3/3) nm and (ii) $Al_{0.1}Ga_{0.9}N$/GaN (4/7) nm QWs grown on GaN-on-Si(111) with different doping levels.[36] (e) CB profile and squared envelope functions of e_1 and e_2 for (i) sample A with 10 nm and (ii) sample B with 15 nm thick step barriers.[37] Reproduced with permission from Kandaswamy *et al.*, Appl. Phys. Lett. **95**, 141911 (2009). Copyright 2009 AIP Publishing LLC. Kandaswamy *et al.*, Appl. Phys. Lett. **96**, 141903 (2010). Copyright 2010 AIP Publishing LLC. Machhadani *et al.*, Appl. Phys. Lett. **97**, 191101 (2010). Copyright 2010 AIP Publishing LLC.

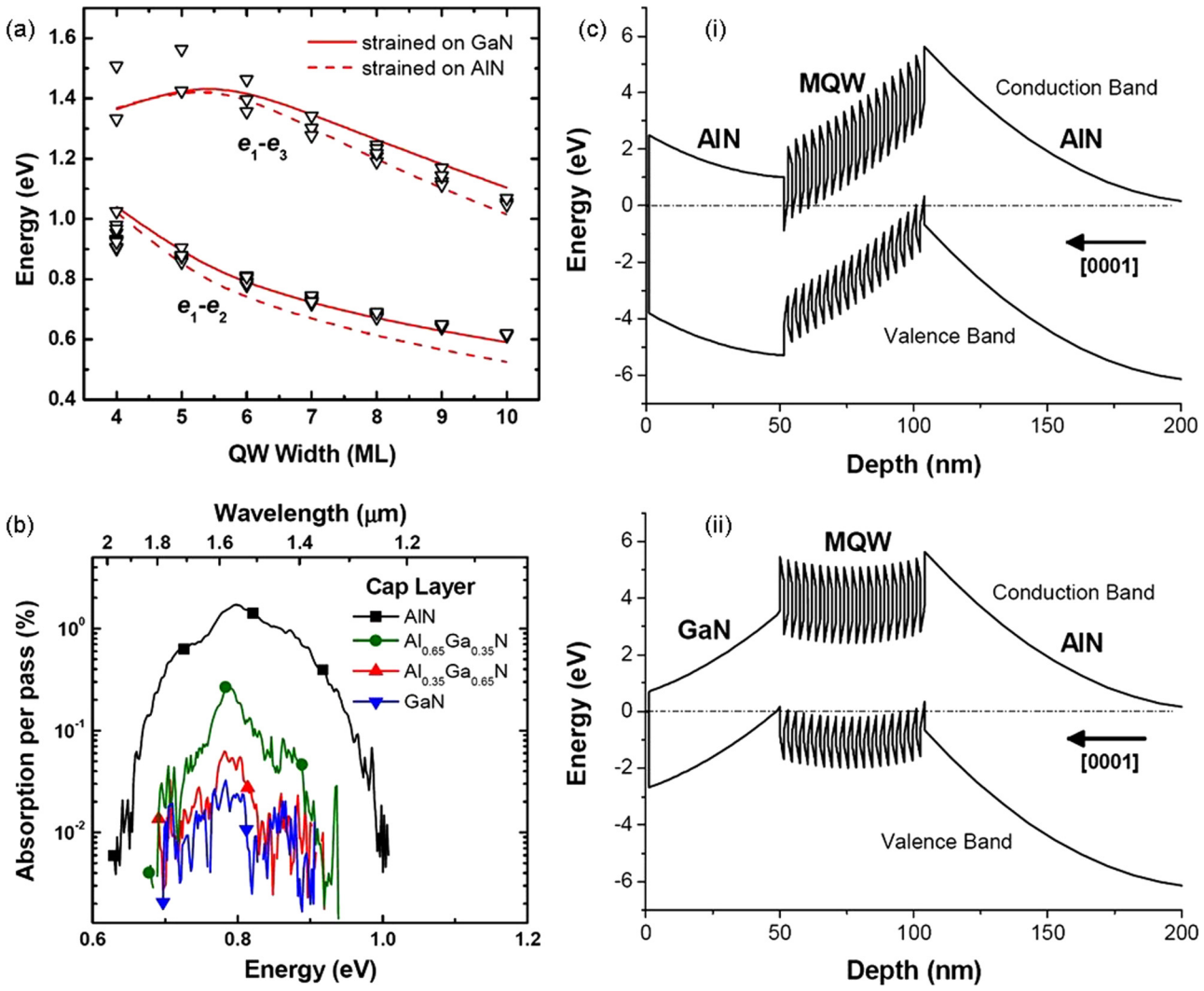

FIG. 3. (a) Variation in the $e_1 - e_2$ and $e_1 - e_3$ ISBT energy as a function of the QW thickness in AlN/GaN SLs with 3 nm thick AlN barriers assuming the structure fully strained on AlN and on GaN, respectively. Experimental data (triangles) and theoretical calculation (solid and dashed lines). (b) Room-temperature TM-polarized ISB absorption spectra of unintentionally doped (UID) AlN/GaN (1.5/1.5) nm MQW structures finished with a 50 nm thick $Al_xGa_{1-x}N$ cap layer with different Al contents. (c) Band diagram of UID AlN/GaN (1.5/1.5) nm MQW structures with (i) AlN cap layer and (ii) GaN cap layer.[38] Reproduced with permission from Kandaswamy *et al.*, J. Appl. Phys. **104**, 093501 (2008). Copyright 2008 AIP Publishing LLC.

high defect scattering will also degrade ISBT. Zhu *et al.*[39] theoretically investigated GaN/InGaN heterostructures for ISBT. This configuration can avoid cracks during the growth due to the compressive strain exhibited by GaN/InGaN MQWs. AlGaN barrier has high alloy disorder and defects scattering, which restricts high-gain photoconductive response from AlGaN/GaN MQWs. In contrast, GaN/InGaN MQWs have significantly reduced alloy disorder and defects scattering in the barrier. Furthermore, the lack of high electron mobility in AlGaN reduces the vertical electron transport across MQWs for electrically driven ISBT applications. However, GaN exhibits much higher electron mobility than AlGaN, improving the vertical electron transport across GaN/InGaN MQWs. Chen *et al.*[40] observed the ISBT in *c*-plane $GaN/In_{0.15}Ga_{0.85}N$ MQWs using growth temperature-controlled epitaxy in MBE. The incorporation of In gave rise to sharp interface restructures with improved ISBT performance. ISBT wavelengths of 3–5 μm range were achieved by varying the QW thickness (T_w) [Figs. 4(a) and 4(b)]. The ISBT peak wavelength first decreased then increased with increasing T_w due to the overlap of the first two electron wavefunction. When $T_w > 2.8$ nm, both e_1 and e_2 were inside the QW [Fig. 4(c)], while when $T_w < 2.8$ nm, only e_1 resided inside the QW [Fig. 4(d)]. In addition, AlInN/GaN

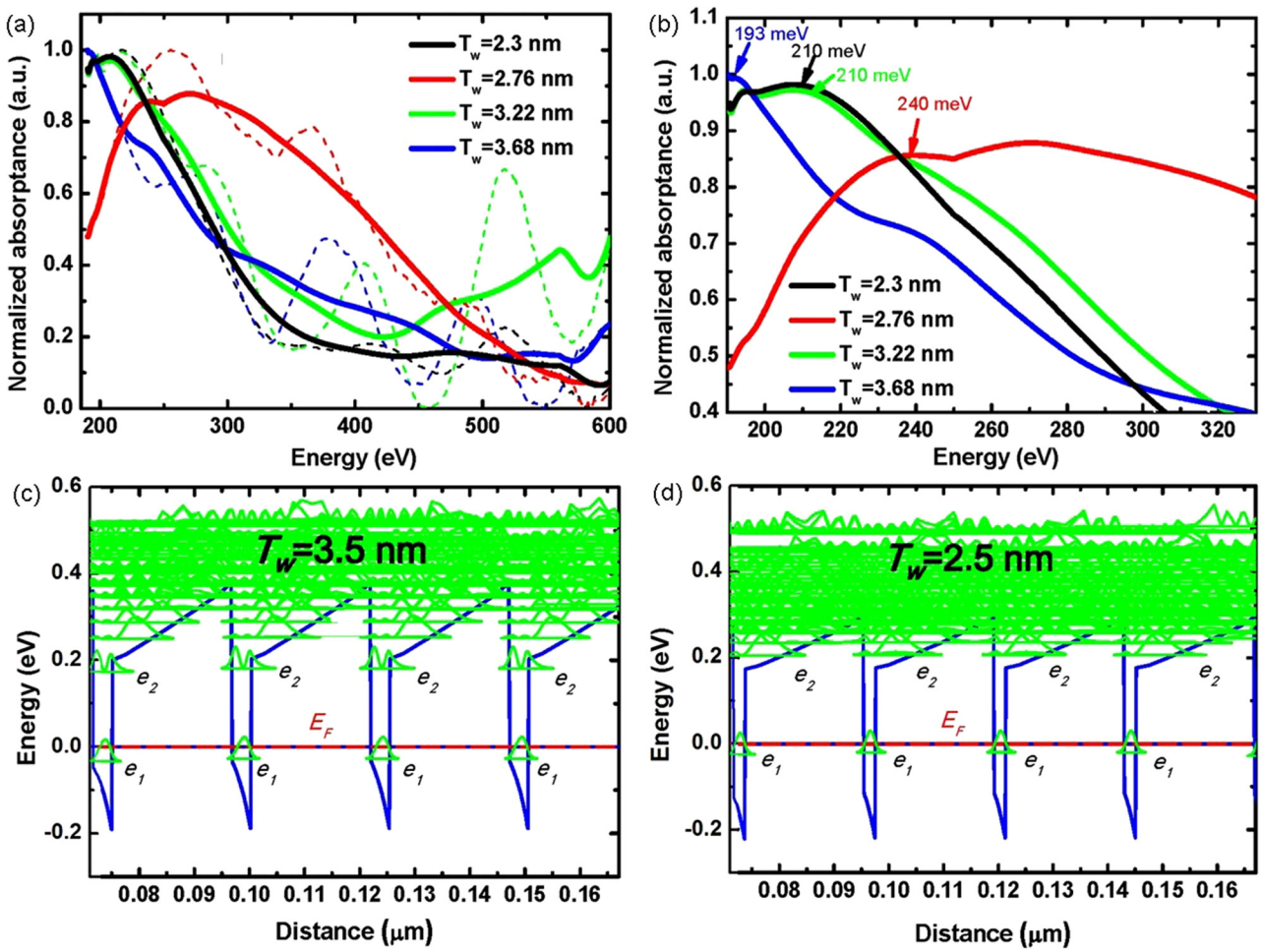

FIG. 4. (a) Normalized absorption spectra (dashed) and their fitted lines (solid) of the GaN/$In_{0.15}Ga_{0.85}N$ MQWs with different well thicknesses. (b) Zoomed fitted absorption spectra. The absorption peaks due to ISBT are labeled. CB profile of GaN/$In_{0.15}Ga_{0.85}N$ (c) (25/3.5) nm MQWs and (d) (25/2.5) nm MQWs.[40] Reproduced with permission from Chen *et al.*, Sci. Rep. **5**, 11485 (2015). Copyright 2015 Springer Nature.

lattice-matched systems have been explored for ISBT. However, due to the limited conduction band offset (~1 eV), only wavelength of >2 μm was observable. Lattice-matched AlInN/GaN SLs were reported to demonstrate ISBT in the 2–4 μm spectral range.[41,42] AlInN/GaInN was also used for ISBT,[43,44] where the In incorporation reduced the formation of cracks during the growth.

D. Cubic GaN

Cubic nitrides do not exhibit polarization effects due to highly symmetric crystal structures. Due to the lack of polarizations, cubic nitrides can access far-IR and THz spectral ranges with a simpler device design. The effective electron mass in cubic GaN is $0.11m_0$, two times smaller than that of wurtzite GaN, which will result in higher gain and lower threshold current density in QCL and QWIPs. A conduction band offset of 1.4 eV and LO phonon energy of 92.7 meV[45] were observed for cubic AlN/GaN heterostructures. DeCuir *et al.*[46] reported near-IR 1.5–2 μm ISB absorption from cubic AlN/GaN SLs and later demonstrated QWIP using AlN/GaN MQWs.[47] Machhandani *et al.*[45] demonstrated ISB absorption in the near-IR to THz spectral range using cubic Al(Ga)N/GaN MQWs. Figure 5(a) shows the ISB absorption spectra of samples A (2/3/100/1×10^{19}), B (3/3/100/1×10^{19}), and C (5/3/100/1×10^{19}), where the numbers inside the brackets represent well thickness (nm), barrier thickness (nm), Al percentage (%), and Si doping (cm^{-3}), respectively. The spectra are fitted with a Gaussian fit with absorption peaks at 1.4, 2.7, and 4.1 μm, respectively. The spectrum broadening was attributed to thickness fluctuations and interface roughness. In contrast, wurtzite (Al)GaN/GaN QWs ISBT spectra are usually fitted by Lorentzian fit, and the spectral broadening was due to multiple factors such as many-body effects and internal field screening.[48] Sample D (12/15/5/2×10^{17}) showed a

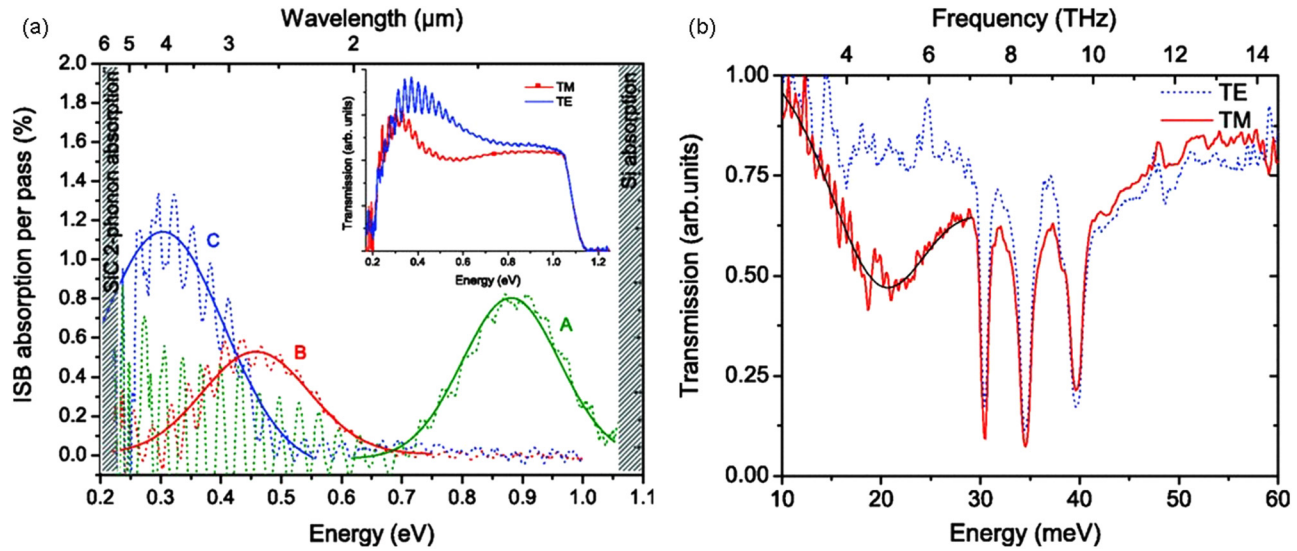

FIG. 5. (a) Room-temperature ISB absorption of samples (a)–(c) (dotted curves) and their Gaussian fits (full curves). Inset: Room-temperature IR transmission spectrum of sample B for TM- and TE-polarized light. (b) Low-temperature far-IR transmission spectrum of sample D for TM-polarized light (solid red) and TE-polarized light (blue dotted). The black solid line is a Gaussian fit of the absorption. The three dominant peaks at 30–40 meV arise from the SiC-on-Si template.[45] Reproduced with permission from Machhadani *et al.*, Phys. Rev. B **83**, 075313 (2011). Copyright 2011 American Physics Society.

peak absorption at 4.76 THz [Fig. 5(b)], which demonstrates cubic III-nitride ISB absorption from telecommunication wavelengths to THz.

E. Quantum dots and wires

Semiconductor QWs are confined along the one direction, leading ISBT electric field component in the out-of-plane *z*-direction, i.e., TM-polarization. QW ISBT that claims to have intrinsic TE-polarization needs to be further verified. In contrast, quantum dots (QDs) are confined in all the three spatial directions with only one polarization, i.e., TE- or TM-polarization.[49] QD density should be around 10^{11}–$10^{12}\,\mathrm{cm}^{-2}$ to observe efficient ISBT.[10] Stranski–Krastanov (SK) growth mode is commonly used to grow Al(Ga)N/GaN QDs in MBE because of three-dimensional island formation due to strain relaxation during the growth. These QDs have a truncated pyramid shape with $\{10\bar{1}3\}$ facets and a hexagonal base.[50] The first observation of ISB absorption in AlN/GaN QDs was reported by Moumanis *et al.*[49] in the range of 1.27–2.4 μm. Tchernycheva *et al.*[51] demonstrated enhanced ISB absorption from doped AlN/GaN QDs in the telecommunications wavelengths of 1.41–1.54 μm. High Si doping and QD density play important roles in efficient ISB absorption. Higher QD density will increase the ISB absorption, while high doping will populate electronic levels with enough electrons for ISBT. The density of QDs was varied by changing the growth interruption time, where high growth interruption time reduced the QD density. Compared with QWs, QDs can be used in photodetectors to enhance responsivity, and they are excellent for high-performance IR detectors for several reasons. First, QDs can produce lower noise in detectors due to reduced electron–phonon scattering. Second, three-dimensional confinement of electrons will decrease thermionic emission and lead to a lower dark current. Third, ISBT in QDs is nearly independent of the polarization of excitation. Most reported III-nitride QD ISBTs are based on Al(Ga)N/GaN QDs. Built-in electric field of AlN/GaN QDs can also provide additional lateral confinement to the localized carries. In terms of AlN/GaN QD SK growth, the QD density is limited to around $10^{10}\,\mathrm{cm}^{-2}$, showing a lack of growth control to achieve higher QD densities required for efficient ISBT. However, recently, it has been demonstrated controlled growth of QD densities between 10^{8} and $10^{11}\,\mathrm{cm}^{-2}$ by changing the growth rate on bulk AlN substrates.[52] To use QDs effectively in active devices, precise control of dot size, uniformity, and composition is necessary. In order to access the telecommunication wavelengths, QD heights should be reduced to ~1 nm. Furthermore, to avoid inhomogenous broadening of the spectrum, QD size fluctuations must also be minimized. For AlGaN/GaN QDs, ISBT redshifted with increasing Al content due to the reduction of conduction band offset, which is in agreement with theoretical predictions.[9]

Semiconductor quantum wires or nanowires (NWs) confine electrons in two spatial dimensions. Longer ISB carrier lifetimes are possible in highly confined systems. Due to the large surface to volume ratio in NWs, misfit strain can be elastically released, expanding the active region size compared with QDs and QWs. Beeler *et al.*[53] demonstrated ISB absorption in self-assembled Ge-doped AlN/GaN NW heterostructures consisting of nano disks (NDs) of alternating AlN and GaN. Two AlN/GaN NWs structures with and without AlN shell were first modeled [Figs. 6(a)–6(c)]. It was found that the incorporation of AlN shell results in a uniaxial strain that blue shifts IB transition. However, it did not have any

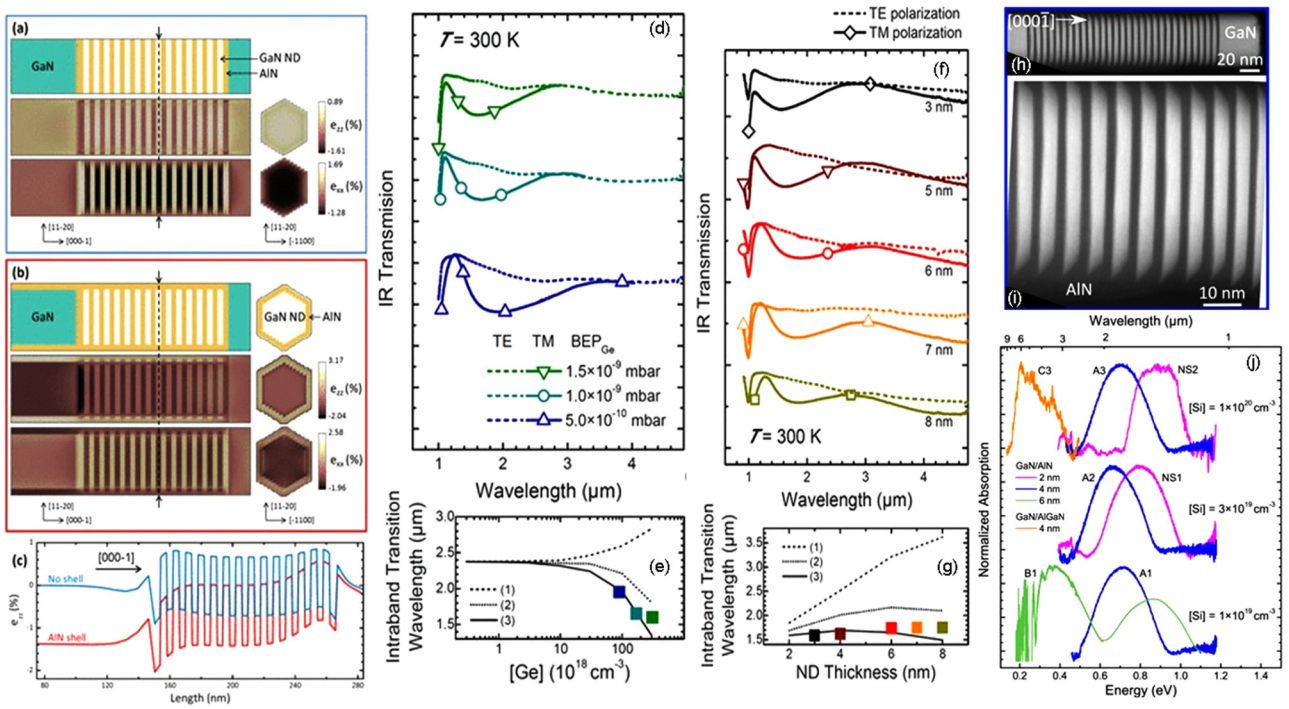

FIG. 6. Simulated structures and cross-sectional views of the e_{zz} and e_{xx} strain components for a NW (a) without and (b) with AlN shell. (c) Comparison of the e_{zz} profile at along ⟨0001⟩ down the center of the NW for both structures. (d) Room-temperature IR transmission spectra for TE-(dashed) and TM-polarized (solid) light measured for Ge-doped AlN/GaN NWs with different doping levels in the GaN NDs. (e) Variation of the ISBT wavelength as a function of Ge concentration. Dots represent experimental values from (d); the dashed line (1) is the calculation of the ISBTs accounting for the screening of the internal electric field; the dotted line (2) incorporates corrections associated with both screening and exchange interaction; the solid line (3) accounts for screening, exchange interaction, and depolarization shift. (f) Room-temperature IR transmission spectra for TE- and TM-polarized light measured for Ge-doped AlN/GaN NWs with different GaN ND thicknesses. (g) Variation of the ISBT wavelength as a function of the ND thickness. Dots represent experimental values from (f); (1)–(3) have similar definition to (e).[53] (h) and (i) HAADF-STEM images of the active region of a NW. (j) Normalized IR absorption for TM-polarized light.[54] (a)–(g) Reproduced with the permission from Beeler *et al.*, Nano Lett. **14**, 1665 (2014). Copyright 2014 American Chemical Society. (h)–(j) Reproduced with permission from Ajay *et al.*, Nanotechnology **29**, 385201 (2018). Copyright 2018 Institute of Physics.

critical effect on ISBTs. AlN/GaN NWs were grown on Si(111) substrates using PAMBE. Ge was incorporated as a *n*-type dopant for NWs without any morphological change to the structures. The dips in TM-polarized IR light were the evidence of the ISB absorption by the NWs, and the dips shifted toward higher wavelengths with decreasing Ge doping [Fig. 6(d)]. Theoretical calculations suggested that internal field screening, exchange interaction, and depolarization shift should be accounted to explain the observed ISBT wavelengths [Fig. 6(e)]. A similar trend was observed in Figs. 6(f) and 6(g), where the dip again shifts toward the higher ISBT wavelengths with increasing GaN ND thickness. Ajay *et al.*[54] recently reported the ISB absorption in AlN/GaN NWs at mid-IR wavelengths on Si(111) substrates using PAMBE with different Si doping and GaN QW widths. Figures 6(h) and 6(i) show the high-angle annular dark-field scanning transmission electron microscopy (HAADF-STEM) of the active region of AlN/GaN NWs. The ISB absorption spectra of the samples were measured using FTIR and plotted in Fig. 6(j). Samples with the same QW width and different Si doping did not show any significant change in the ISB absorption. However, ISB absorption shifted to lower energies with increasing QW width. $Al_{0.4}Ga_{0.6}N$ NWs with low Si doping concentrations ($<1\times10^{20}$ cm^{-3}) did not show any ISB absorption since the ISB absorption is weak and spectra linewith broadens, reducing the peak intensity at low doping. Two factors may be attributed to this observation. First, alloy inhomogeneity in the barrier material (in comparison with AlN/GaN) contributes to an additional dispersive element to the spectrum, reducing the peak intensity and avoiding the detection of any ISB absorption. Second, ISB absorption of $Al_{0.4}Ga_{0.6}N$ NWs is in the vicinity of the second-order reststrahlen band of GaN, which attenuates the ISB absorption due to phonon-related absorption. In such instances, higher doping is required to identify the ISB absorption. Overall, doping concentration and QW width in NWs have a strong impact on ISBT.

In short summary, III-nitrides based ISBT can cover near-IR to THz wavelengths. Table I summarizes ISBTs with different structures, where most of them are centered around the telecommunication wavelength of 1.55 μm. By changing the active region width, barrier, Al composition, and doping, other wavelengths are also accessible in some of the structures.

TABLE I. III-nitrides based ISBT with different structures.

ISBT system (material/structure)	Thickness well/barrier (nm) (or QD density cm^{-2})	Well doping (cm^{-3})	Spectral range (μm)	Reference
$Al_xGa_{1-x}N$/GaN MWQs $x = 0.65$ and 0.85	0.6/0.11–0.13	1×10^{20}	1.41–1.7	29
$Al_xGa_{1-x}N$/GaN SLs $x = 0.1$ and 1.0	3.0–7.0/3–4	5×10^{19}	2–9	35
$Al_{0.05}Ga_{0.95}/Al_{0.1}Ga_{0.9}$/GaN step barrier QWs	3.0/10–15 (step)/3.0	$0.5–1 \times 10^{19}$	70–143	37
Cubic AlGaN/GaN MQWs	2.0–12.0/3.0–15.0	$0.02–5 \times 10^{19}$	1.4–63	45
AlN/GaN QDs	$1–3 \times 10^{-11}$	5×10^{16}	1.27–2.4	49
AlN/GaN QDs	$0.1–2.9 \times 10^{-12}$	UID-1×10^{20}	1.41–1.54	51
AlN/GaN NDs in GaN NWs	3–8/4	$1.5–2.4 \times 10^{20}$	1.75–1.95	53
AlN/GaN and $Al_{0.4}Ga_{0.6}N$/GaN heterostructures in GaN NWs	1.7–5.7/3.0	$0.3–1 \times 10^{20}$	1.4–3.4	54
m-, *a*-plane AlGaN/GaN MQWs	3.0–3.7/3.0	1.2×10^{19}	3.8–5.6	56
$(11\bar{2}2)$-AlN/GaN QWs	1.2–3.0/3–5	5×10^{19}	1.5–4.5	62

IV. EFFECTS OF CRYSTAL ORIENTATION AND DOPING ON ISBT

A. Crystal orientation dependence

Crystal orientation-dependent ISBTs were theoretically studied in semipolar AlGaN/GaN single QW (SQW) for optoelectronic applications.[22] ISBT frequency, dipole matrix elements, and absorption spectra were calculated for $0° < \theta < 90°$, where θ is the inclination angle of the crystal plane from the *c*-plane in comparison with polar *c*- ($\theta = 0°$) and nonpolar *m*- ($\theta = 90°$) planes. The QWs were undoped to understand the polarization effects without complications caused by doping such as band tilting. As shown in Fig. 1, $(20\bar{2}1)$ and *m*-planes show a relatively flat conduction band profile with a large overlap of the sub-band wavefunctions. However, *c*- and $(10\bar{1}3)$ planes showed tilted band profile with a reduced wavefunction overlap, which will affect dipole matrix, ISBT frequency, and absorption coefficient. Figure 7(a) shows ISBT frequency and matrix element as a function of crystal orientations of AlGaN/GaN QW. The ISBT frequency decreased with increasing θ and remained almost constant after 55°, which is directly related with the polarization effects. In region I ($0° < \theta < 45°$), piezoelectric polarization is dominant and becomes zero at $\theta = 45°$, whereas in region II ($45° < \theta < 70°$), both spontaneous and piezoelectric polarizations are important. In region III ($70° < \theta < 90°$), total polarization is very close to zero. When $\theta > 55°$, total polarization is small enough and has negligible effects on the QW band structure profile. The matrix element shows the opposite trend to the ISBT frequency characteristics, indicating a higher wavefunction overlap and absorption coefficient at $\theta > 55°$. Figure 7(b) shows absorption spectra for *c*-, *m*-, and semipolar planes. When the angle θ increased, the spectra moved toward that of the *m*-plane. Therefore, the nonpolar and

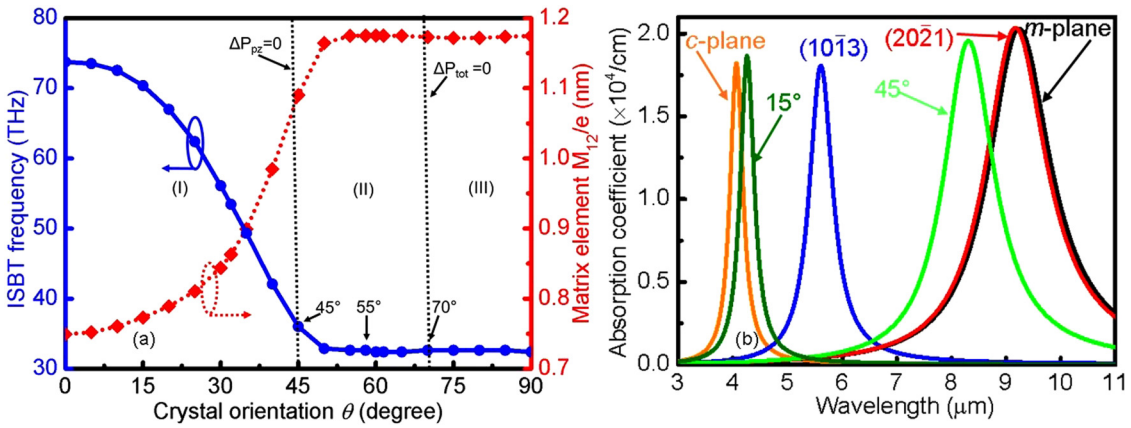

FIG. 7. (a) ISBT frequency and matrix element (M_{12}/e) of $Al_{0.3}Ga_{0.7}N$/GaN (25/5) nm SQW structures on various semipolar plane orientations. The first dashed line is at $\theta = 45°$ where piezoelectric polarization $\Delta P_{pz} = 0$; and the second dashed line is at $\theta = 70°$ where the total polarization $\Delta P_{tot} = 0$. Three regions (I)–(III) are defined by the two dashed lines. (b) Absorption spectra for AlGaN/GaN SQW on different planes, including *c*-plane, *m*-plane, and four semipolar planes.[22] Reproduced with permission from Fu *et al.*, J. Appl. Phys. **119**, 174502 (2016). Copyright 2016 AIP Publishing LLC.

semipolar planes with $\theta > 55°$ are favorable for long wavelength with high absorption.

Several case studies were performed for *c*-, (10$\bar{1}$3), (20$\bar{2}$1), and *m*-planes to study the effects of QW thickness, barrier thickness, and barrier Al composition on ISBT. The ISBT frequency decreased with increasing the QW for *m*-, (20$\bar{2}$1), and (10$\bar{1}$3) planes, while the *c*-plane showed almost constant ISBT frequency regardless of the QW width. Due to the weak polarization effects, the (20$\bar{2}$1) plane can be approximated as a finite square potential well, in which transition energy is inversely proportional QW width squared. In contrast, the (10$\bar{1}$3) plane experiences large polarization-related effects, leading to titled QW profile and limited sub-band wavefunctions separation. Therefore, the semipolar (20$\bar{2}$1) plane have tunable ISBT frequency by changing QW width, whereas the semipolar (10$\bar{1}$3) plane is limited with achievable frequencies. Figures 8(a)–8(c) shows the absorption spectra from the above two semipolar planes in comparison with the *c*-plane for different QW thicknesses. For *c*- and (10$\bar{1}$3) planes, the spectra concentrated at a narrow wavelength range and showed negligible movement with the QW thickness. But for the (20$\bar{2}$1) plane, the wavelength was dispersive in the large wavelength range. Figures 8(d)–8(f) demonstrate the absorption spectra with wavelengths for the planes of interest *c*-, (10$\bar{1}$3), and (20$\bar{2}$1) for different barrier thicknesses. Thick barriers strongly affected the ISBT properties of the QWs on *c*- and (10$\bar{1}$3) planes, while (20$\bar{2}$1) and *m*-planes are immune to barrier thickness variation. The similar phenomenon was observed when varying barrier Al composition. In short, semipolar GaN/AlGaN QWs with weak polarization effects ($55° < \theta < 90°$) have tunable transition frequencies and long-wavelength responses with high absorption and immunity to barrier thickness and Al composition fluctuations.

B. Modulation doping effects

Fu *et al.*[55] theoretically investigated the modulation doping effects on ISBT properties of semipolar AlGaN/GaN SQW. Three doping schemes were studied, including QW doping, barrier continuous doping, and barrier δ-doping [Figs. 9(a)–9(c)]. In both planes, for all the doping schemes, peak absorption wavelengths moved toward higher wavelengths with increasing doping concentration. As shown in Fig. 9(d), peak absorption wavelength showed a strong dependence for the (20$\bar{2}$1) plane and a weak dependence for the (10$\bar{1}$3) plane with the doping density. The δ-doping showed the strongest influence for the (20$\bar{2}$1) plane, followed by QW doping and barrier doping. This indicates that δ-doping is beneficial for long-wavelength devices with reduced carrier and impurity scattering in the QW layer. Figures 9(e)–9(j) explain the absorption wavelength shift for both planes for different doping schemes. For the (20$\bar{2}$1) structure, higher doping will induce large band bowing and reduced effective barrier height ($E_{B,eff}$), leading to smaller sub-band energy difference and increased absorption wavelength. δ-doping showed the largest band bowing compared with QW and barrier doping. However, band bending in (10$\bar{1}$3) was complicated by large polarization charges. For (10$\bar{1}$3) SQWs, the

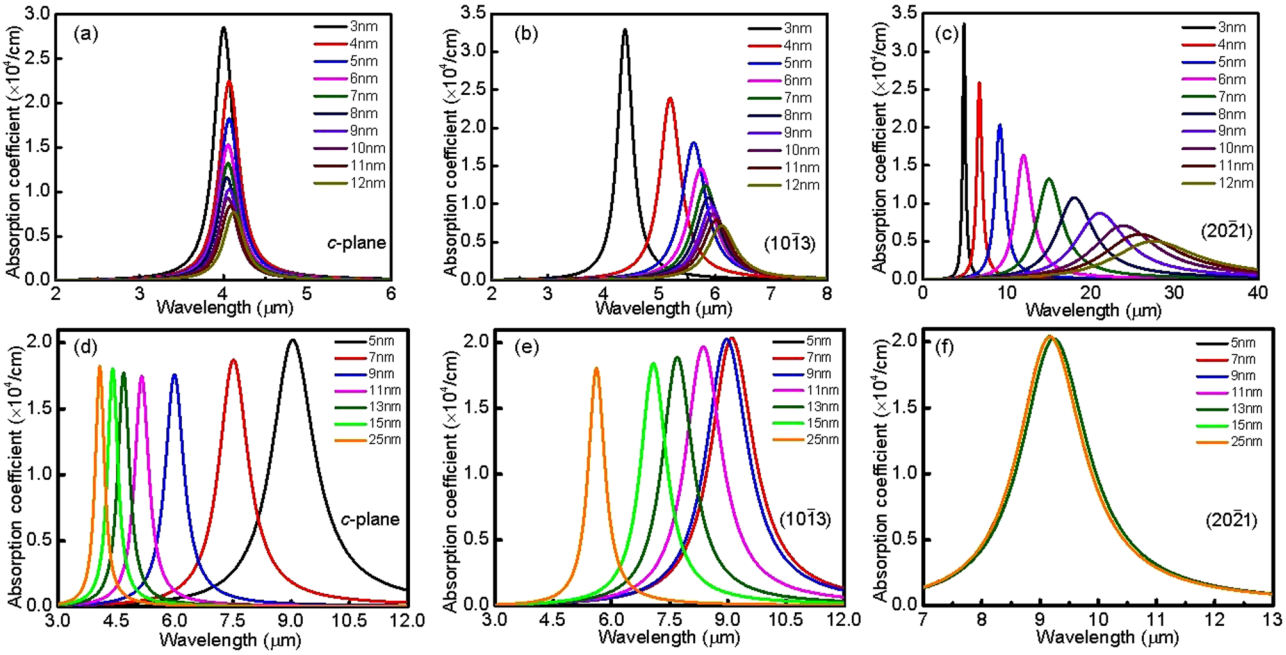

FIG. 8. Absorption spectra of (a) *c*-plane, (b) (10$\bar{1}$3), and (c) (20$\bar{2}$1) (25 nm) $Al_{0.3}Ga_{0.7}N$/GaN SQW varying QW thickness from 3 to 12 nm. Absorption spectra of (d) *c*-plane, (e) (10$\bar{1}$3), and (f) (20$\bar{2}$1) $Al_{0.3}Ga_{0.7}N$/GaN (5 nm) SQW varying barrier thickness from 5 to 25 nm.[22] Reproduced with permission from Fu *et al.*, J. Appl. Phys. **119**, 174502 (2016). Copyright 2016 AIP Publishing LLC.

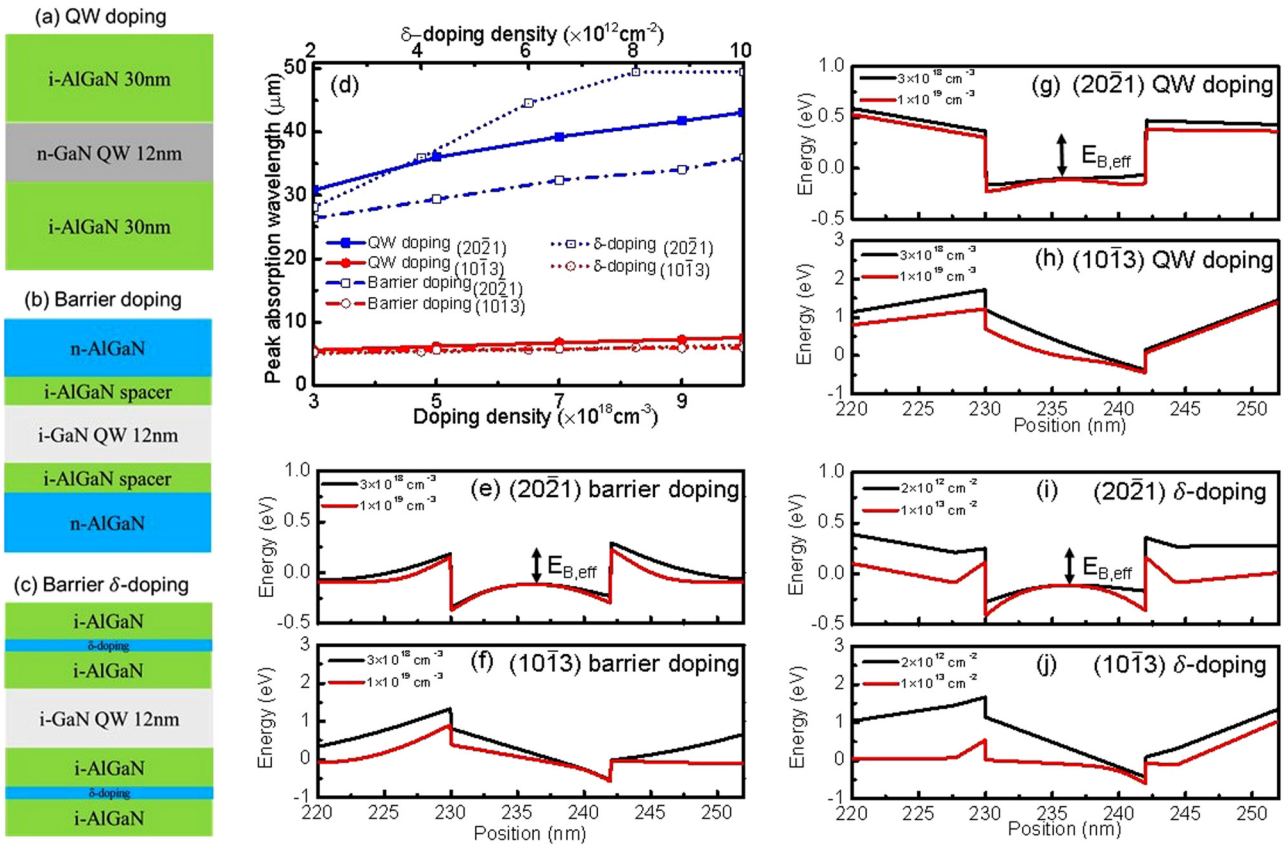

FIG. 9. Schematics of three different doping schemes: (a) QW doping, (b) barrier doping, and (c) barrier δ-doping. (d) The peak absorption wavelength as a function of doping density for (20$\bar{2}$1) and (10$\bar{1}$3) QWs under three doping schemes. (e)–(j) CB of (20$\bar{2}$1) and (10$\bar{1}$3) QWs under three doping schemes at high and low doping densities.[55] Reproduced with permission from Fu *et al.*, J. Appl Phys. **121**, 014501 (2017). Copyright 2017 AIP Publishing LLC.

band tilting is present regardless of the doping concentrations, explaining the small variation in absorption wavelength.

Barrier doping can tune ISBT wavelength while keeping the impurities away from the QW. The spacer thickness in barrier doping also plays a key role. Figures 10(a) and 10(b) show the absorption coefficients for both (20$\bar{2}$1) and (10$\bar{1}$3) planes with different spacer thicknesses. For the (20$\bar{2}$1) plane, peak absorption coefficients increased, and the peak absorption wavelengths decreased with increasing spacer thickness. For the (10$\bar{1}$3) plane, both peak absorption coefficients and wavelengths decreased with increasing spacer thickness. Furthermore, the position of the δ-doping is also critical, similar to the spacer thickness in barrier doping. The advantage of δ-doping is that high doping concentration without degrading the material quality. For the (20$\bar{2}$1) QW, the peak absorption coefficient increased while the peak absorption wavelength reduced as the δ-doping is moving away from the QW. For the (10$\bar{1}$3) plane, peak absorption coefficients and wavelengths decreased with increasing δ-doping position [Figs. 10(c) and 10(d)]. δ-doping is more effective in achieving longer absorption wavelength than barrier doping. This is because the centroid of the donor charges in δ-doping is much closer to the QW than that of barrier doping when the distance between the edge of barrier donor and QW is the same. In short, modulation doping can strongly alter ISBT properties of semipolar AlGaN/GaN QWs.

C. Nonpolar and semipolar ISBT

To date, there are few reports on the experimental demonstration of nonpolar *m*- and *a*-plane ISBT. Monavarian *et al.*[56] investigated mid-IR transitions in *m*- and *a*-plane MQWs [Fig. 11(a)] grown by ammonia MBE (NH_3-MBE). NH_3-MBE can provide controllable and abrupt interfaces. They systematically studied the effects of QW widths and doping profiles. Two doping schemes were employed to study the modulation doping effect, i.e., well-doped (WD) and barrier-doped (BD). Figure 11(b) shows the experimental set-up used to measure the ISB absorption and the obtained spectra are in Fig. 11(c). The calculated conduction band diagram with band bowing due to the barrier doping can be seen in Fig. 11(d). Figures 11(i) and 11(j) show the HAADF-STEM images for *m*- and *a*-plane MQWs. Higher interface roughness can

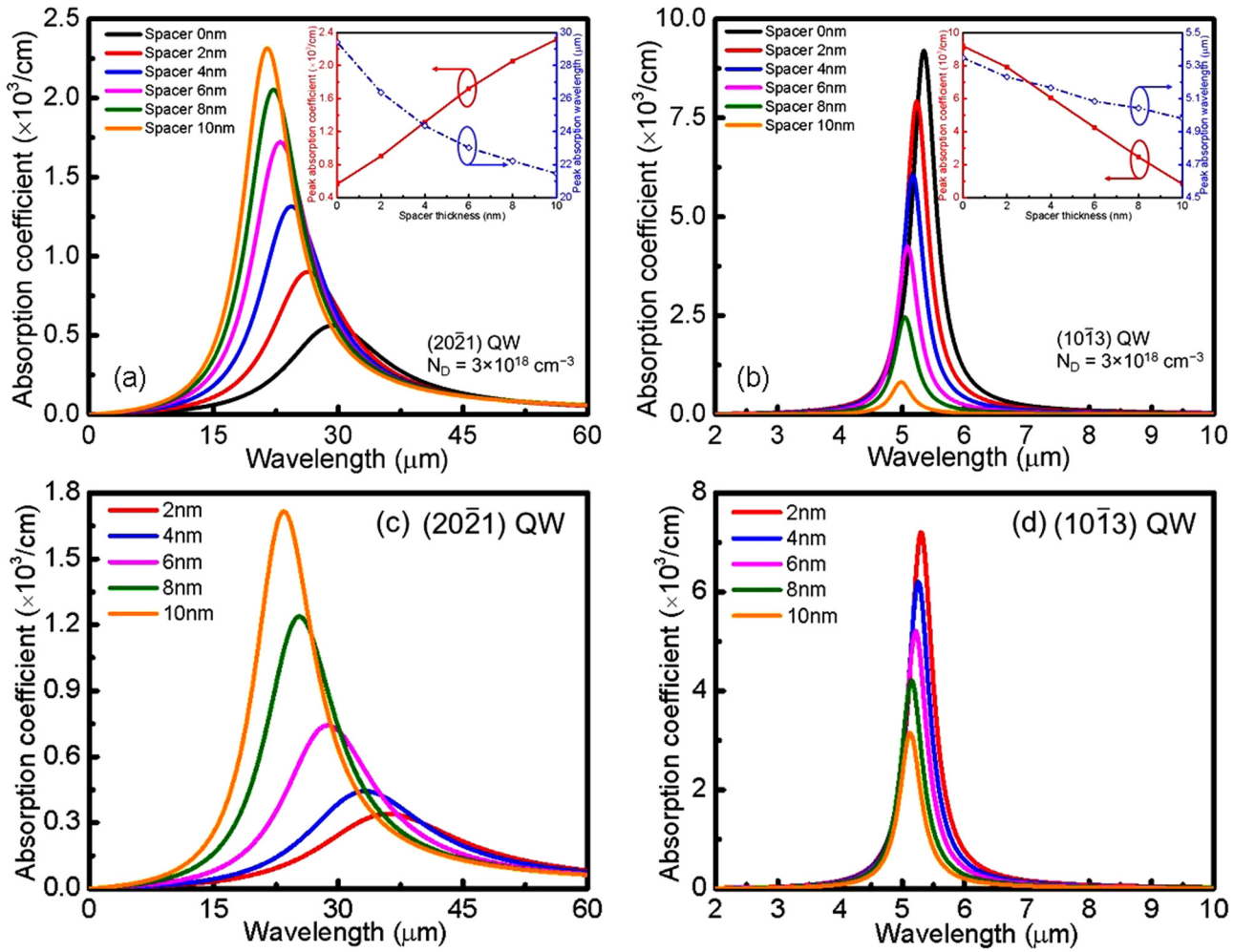

FIG. 10. Absorption spectra of (a) (20$\bar{2}$1) QWs and (b) (10$\bar{1}$3) QWs with spacer thickness ranging from 0 to 10 nm under the barrier doping scheme with doping density of 3×10^{18} cm^{-3}. Insets: Peak absorption coefficient and wavelength as a function of the spacer thickness. Absorption spectra of (c) (20$\bar{2}$1) QWs and (d) (10$\bar{1}$3) QWs with different δ-doping positions.[55] Reproduced with permission from Fu *et al.*, J. Appl Phys. **121**, 014501 (2017). Copyright 2017 AIP Publishing LLC.

be observed on the *a*-plane structures when compared to the *m*-plane structure due to the higher stability of the *m*-plane. Figures 11(e)–11(h) show the ISB absorption spectra for BD and WD structures. The ISBT energy increased with decreasing QW thickness decrease, which is consistent with quantum mechanics. For both planes, WD structures showed slightly lower ISBT energies compared with BD structures. It should be noted that no significant difference in ISB absorption linewidth was observed for both WD and BD structures with only small dependence of ISB linewidth on the QW width. Lim *et al.*[57] reported *m*- and *a*-plane AlN/GaN MQW grown by PAMBE. *m*-plane structures had better mosaicity, surface roughness, photoluminescence (PL) linewidth and intensity, and ISB absorption in contrast with *a*-plane structures. The absence of internal electric fields in nonpolar planes enhanced accessible spectral range and efficiency for ISBTs.[58–61]

Despite the reduced polarization effects and improved performance, semipolar structures suffer from growth challenges, and most of the reported results are on the (11$\bar{2}$2) semipolar plane with a relatively small polarization effect. Machhadani *et al.*[62] reported AlN/GaN MQWs grown on (11$\bar{2}$2) GaN with different QW thicknesses and absorption spectral range of 1.5–4.5 μm. Figure 12(a) shows the absorption spectra for both semipolar and polar structures, and Fig. 12(b) shows the peak ISB absorption energy as a function of QW thickness. The semipolar QWs exhibited a large peak energy shift with increasing QW thickness compared the polar *c*-plane QWs due to reduced polarization field. The ISB absorption had a Gaussian profile due to QW width variation and stacking faults. Figure 12(c) demonstrates the simulated band profile for both polar *c*- and (11$\bar{2}$2) semipolar planes. In *c*-plane QW, the electron wavefunctions are limited to the triangular shape

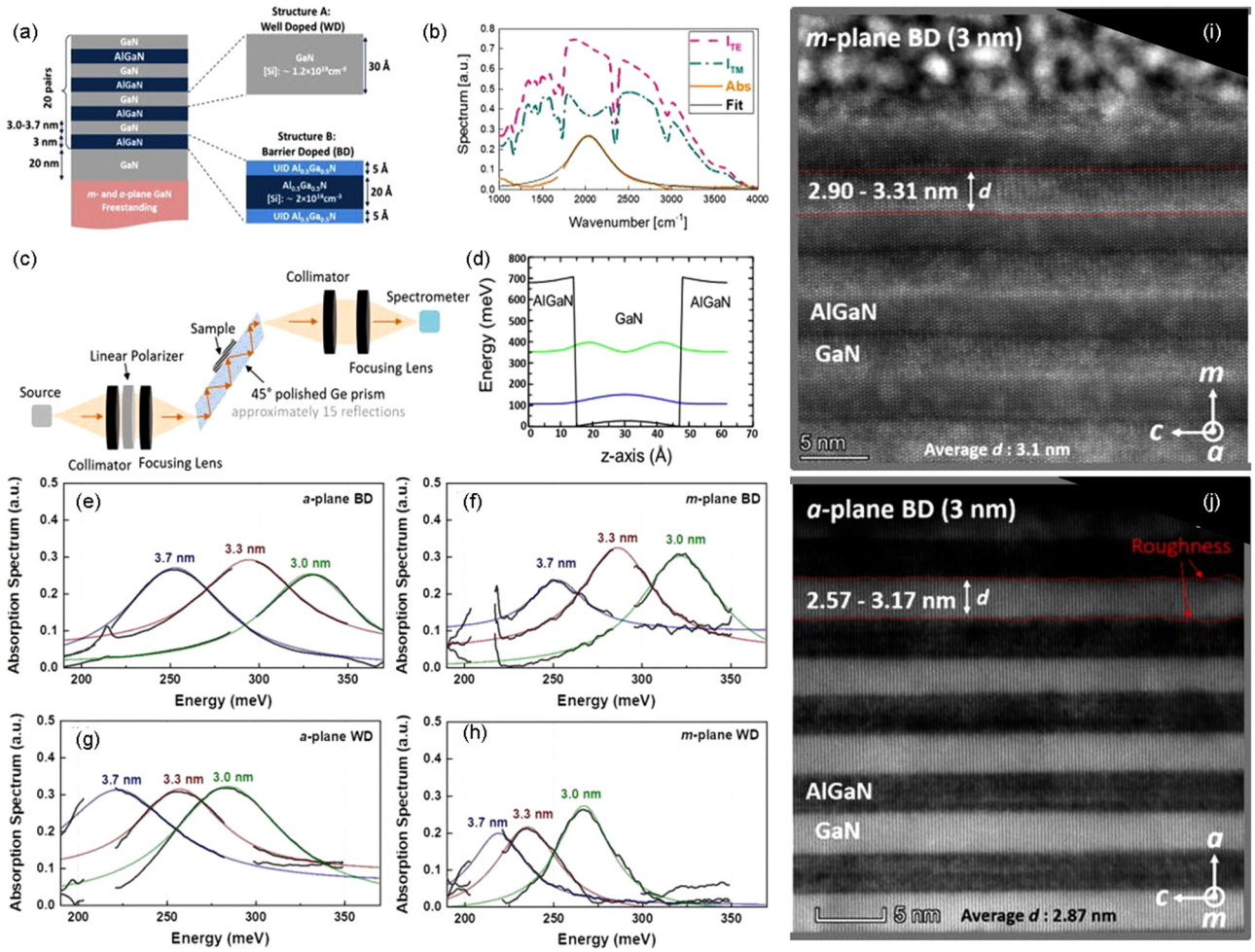

FIG. 11. (a) Cross section of nonpolar *m*-plane and *a*-plane heterostructures with WD and BD configurations. (b) ISB absorption measurement set-up. (c) Experimental data obtained in the set-up in (b). (d) Calculated CB diagram and squares of electron wavefunctions for the first two states of BD 3.3 nm wide $Al_{0.5}Ga_{0.5}N$/GaN QW structures. ISB absorption spectra of (e) *a*-plane BD, (f) *a*-plane WD, (g) *m*-plane BD, and (h) *m*-plane WD $Al_{0.5}Ga_{0.5}N$/GaN MQW structures. HAADF-STEM images of (i) nonpolar *m*-plane and (j) *a*-plane BD heterostructures.[56] Reproduced with permission from Monavarian *et al.*, Appl. Phys. Lett. **116**, 201103 (2020). Copyright 2020 AIP Publishing LLC.

region of the band profile; therefore, increasing QW width has minimal effect on the wavefunctions. For the semipolar $(11\bar{2}2)$ QW with a flatband profile, the energy difference between the first two sub-bands decreases with increasing QW width. Lahourcade *et al.*[63] reported IB and ISB optical properties of semipolar $(11\bar{2}2)$ AlN/GaN MQWs on sapphire substrates by PAMBE. The devices showed reduced transition energies for both IB and ISB with increasing QW thickness [Figs. 12(d) and 12(e)], which is consistent with previous observation.

V. III-NITRIDE ISBT DEVICES AND APPLICATIONS

A. Photodetectors

QWIP works on the principle of ISB absorption under IR radiation, where the electrons are photoexcited from the ground state to the electron continnum under an applied bias. As a result, a photocurrent is generated and can be measured according to the intensity of light and the bias voltage. Hofstetter *et al.*[8] demonstrated the first AlN/GaN QWIP with a photoresponse of 0.1 mA/W at 10 K and peak wavelength of 1.76 μm. Sudradjat *et al.*[64] reported AlGaN double step QW design for the detection of far-IR radiation peaking at 13 THz (23 μm) at 50 K with ~7 mA/W responsivity. Baumann *et al.*[65] showed a AlN/GaN QWIP at 1.6 μm with high-temperature operation of 120 K. Usually, the photocurrent is reduced at higher temperatures due to large dark currents caused by defect mediated leakage paths. With the advancement of high-quality material growth, low-defect room-temperature QWIPs were reported.[66–68] Durmaz *et al.*[69] demonstrated THz QWIP on AlGaN/GaN MQWs grown on the semipolar $(20\bar{2}1)$ GaN substrate by MBE. Figure 13(a) shows the conduction band diagram of the

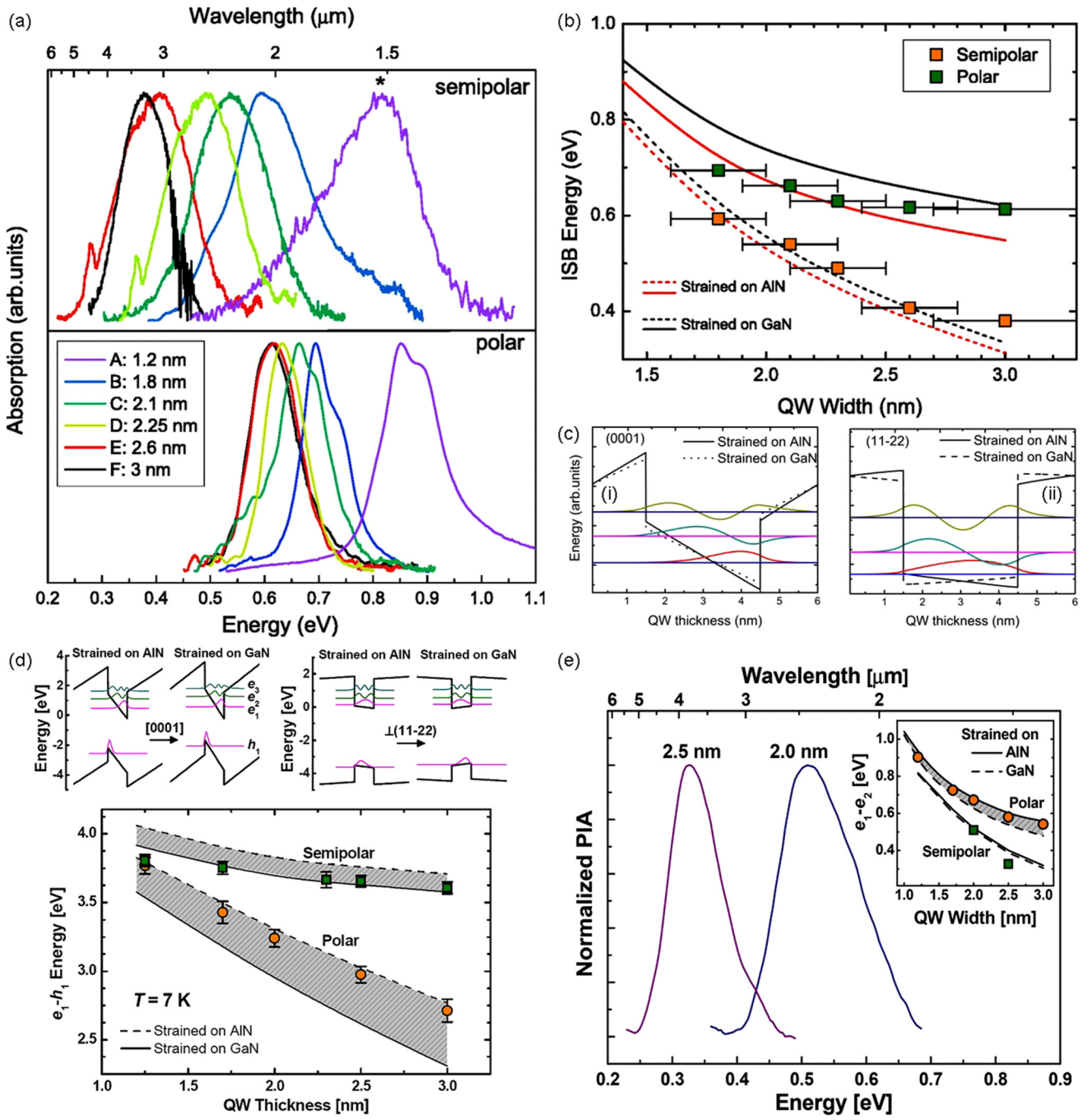

FIG. 12. (a) ISB absorption spectra for semipolar (top) and polar (bottom) AlN/GaN QWs with different well thicknesses. The spectrum labeled with a star has been obtained by photoinduced absorption (PIA) measurement. (b) Calculated and measured ISB absorption energy vs well thickness. (c) CB diagram of (i) (0001)- and (ii) $(11\bar{2}2)$-oriented AlN/GaN (3/3) nm QWs in a SL. Solid lines and dashed lines correspond to simulations assuming the SL strained on AlN and on GaN, respectively.[62] (d) Band diagram of (0001)- and $(11\bar{2}2)$-oriented AlN/GaN (5/2.5) nm MQWs assuming the structure is fully strained on AlN and on GaN, respectively (top). Evolution of $e_1 - h_1$ as a function of the QW thickness and strain state (bottom). The dots represent experimental measurements. (e) Room-temperature PIA spectra for TM-polarized light measured in $(11\bar{2}2)$-oriented AlN/GaN MQWs with 3 nm thick AlN barriers and GaN QWs with thicknesses of 2 and 2.5 nm. Inset: Calculated ISB energy for semipolar and polar structures. The dots represent experimental measurements.[63] Reproduced with permission from Machhadani *et al.*, J. Appl. Phys. **113**, 143109 (2013). Copyright 2013 AIP Publishing LLC. Lahourcade *et al.*, Appl. Phys. Lett. **93**, 111906 (2008). Copyright 2008 AIP Publishing LLC.

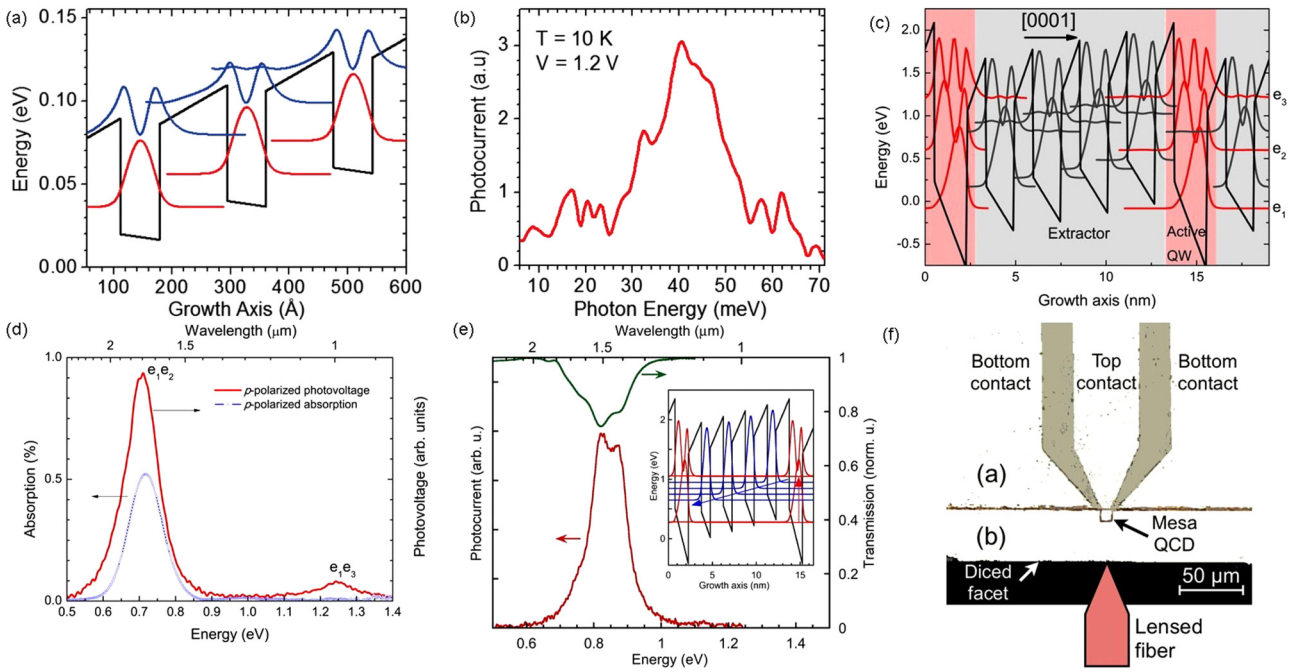

FIG. 13. (a) CB diagram of the semipolar AlGaN/GaN QWIP under an externally applied voltage bias of about 20 mV/period and the squared envelope functions of subbands of each well referenced to their respective energy levels. (b) Photocurrent spectrum measured at 10 K under an applied voltage of 1.2 V.[69] (c) CB diagram of one period of the QCD with the adjacent active QW. The red and gray regions correspond to the active QW and the extractor stage, respectively. (d) Absorption and photovoltage spectra under *p*-polarized light.[78] (e) Room-temperature photocurrent spectrum of $700 \times 700\,\mu m^2$ QCD and transmission spectrum of the QCD sample. Inset: CB diagram and squared envelope functions of one QCD period. (f) Top-view optical microscope image of a $10 \times 10\,\mu m^2$ QCD device.[79] Reproduced with permission from Durmaz *et al.*, Appl. Phys. Lett. **108**, 201102 (2016). Copyright 2016 AIP Publishing LLC. Sakr *et al.*, Appl. Phys. Lett. **100**, 181103 (2012). Copyright 2012 AIP Publishing LLC. Sakr *et al.*, Appl. Phys. Lett. **102**, 011135 (2013). Copyright 2013 AIP Publishing LLC.

QWIP with a relatively flat QW profile due to the weak polarization effects in the $(20\bar{2}1)$ semipolar plane. The ISBT energy between the first two electron wavefunctions was calculated to be 42.8 meV, which is 10.3 THz in frequency and 29.0 μm in wavelength. The photocurrent spectrum was measured at $T = 10$ K at a bias of 1.2 V using FTIR spectroscopy [Fig. 13(b)]. Using a Gaussian fit, the peak energy was 41.7 meV, which corresponds to 10.1 THz and 29.7 μm and is in excellent agreement with calculated values. These results show that semipolar GaN plane can be developed for QWIP in THz spectral range. Hofstetter *et al.*[70] showed that responsivity could be enhanced 60 times by replacing AlN/GaN QWs with QDs at 160 K. First, QDIPs were demonstrated by Doyennette *et al.*[71] with peak detection wavelength of 1.38 μm at 77 K. In follow-up work, Doyennette *et al.*[72] demonstrated ISB photodetection of self-organized AlN/GaN quantum dots at 1.3–1.5 μm. Vardi *et al.*[73] observed the first demonstration of room-temperature ISB photodetection using AlN/GaN QDIP with a peak responsivity of 8 mA/W at 1.41 μm.

Unlike the QWIPs or QDIPs, QCDs can be considered as ISBTs based photovoltaic devices that operate under zero bias. QCDs do not have dark current at zero bias, which is suitable for large signal to noise ratios and low intrinsic capacitance for high frequency operation. A QCD consists of two stages: a QW region that absorbs light using ISB absorption and excites electrons and an extractor stage that collects the exited electrons. QCDs can generate an open-circuit voltage or a photocurrent if connected to a load. Vardi *et al.*[74] reported the first AlGaN/GaN/AlN ISB absorption based QCD and later high-speed operation of a AlGaN/GaN QCD at 1.55 μm.[75] Song *et al.*[76] reported MOCVD grown $Al_{0.5}Ga_{0.5}N$/GaN QCD that operated at around 4 μm with a responsivity ~100 μA/W. Sarkr *et al.*[77] demonstrated a simplified AlGaN/GaN QCD with an AlGaN thick layer extractor. The same group developed[78] two-color AlGaN/GaN QCD at short IR wavelengths of 1.0 and 1.7 μm. Figure 13(c) shows the active region and extractor region of the detector, and Fig. 13(d) represents the ISB absorption and open-circuit voltage (photovoltage) of the detector. Two photovoltage peaks were observed at 1 and 1.7 μm, which correspond to $e_2 - e_1$ and $e_3 - e_1$ ISBT, respectively. Later Sarkr *et al.*[79] reported a AlGaN/GaN QCD that can operate at ~40 GHz bandwidth at 1.55 μm wavelength, as shown in Fig. 13(e). Figure 13(f) represents $10 \times 10\,\mu m^2$ QCD device coupled with a fiber optic coupled continuous-wave laser diode that operates at 1.55 μm wavelength. The device showed a room-temperature responsivity of 9.5 mA/W and 42 GHz at −3 dB bandwidth due to the reduced intrinsic capacitance. This work highlights the possibility of AlGaN/GaN material systems for ultrafast QCDs covering not only near-IR but also mid-IR to THz spectral regions.

B. Quantum cascade lasers

Lasing through the ISBT process in III-nitrides remains quite challenging. Currently, GaAs devices are mainly used for THz QCL.[80] However, most of them can only be operated at cryogenic temperatures due to the low LO phonon energy. Thermal backfilling and thermally activated phonon scattering are the root causes for degradation of population inversion at high temperatures for GaAs devices.[9] Nevertheless, with improved device designs, THz QCLs with operation temperatures of 210[81] and 250 K[82] have been demonstrated by ETH Zürich and MIT, respectively. Recently, III-nitride based QCLs have attracted considerable interest because GaN has a large LO phonon energy of 92 meV (22 THz), which is promising for room-temperature THz QCLs.[83] To date, the development of GaN based THz QCLs is still under way. Some reports of THz emission form III-nitrides are summarized below. Most of the demonstrated devices have the resonant phonon (RP) type QCL structures [Fig. 14(c)]. Based on theoretical simulation of GaN based QCLs,[84–87] Terashima and Hirayama[88] reported 7.6 THz emission from the $In_{0.05}Al_{0.23}Ga_{0.72}N$/GaN QC structure [Fig. 14(a)] and 7.5 THz emission from the $Al_{0.2}Ga_{0.8}N$/GaN four well module QC structure.[89] In Fig. 14(b), sharp interfaces between wells and barriers can be observed with minimal thickness fluctuations. Observation of emission of 1.37 THz using AlGaN/GaN based QCL was reported.[90] Terashima and Hirayama[91] further reported excellent sample morphology and material characterizations on the AlGaN/GaN QCL structure on the AlGaN template. In 2015, Song *et al.*[92] observed light emission from the $Al_{0.65}Ga_{0.35}N$/GaN QC structure [Fig. 14(c)] with a peak wavelength of 4.9 μm and a full width at half maximum (FWHM) of about 100 meV [Fig. 14(d)]. This QC structure was designed with

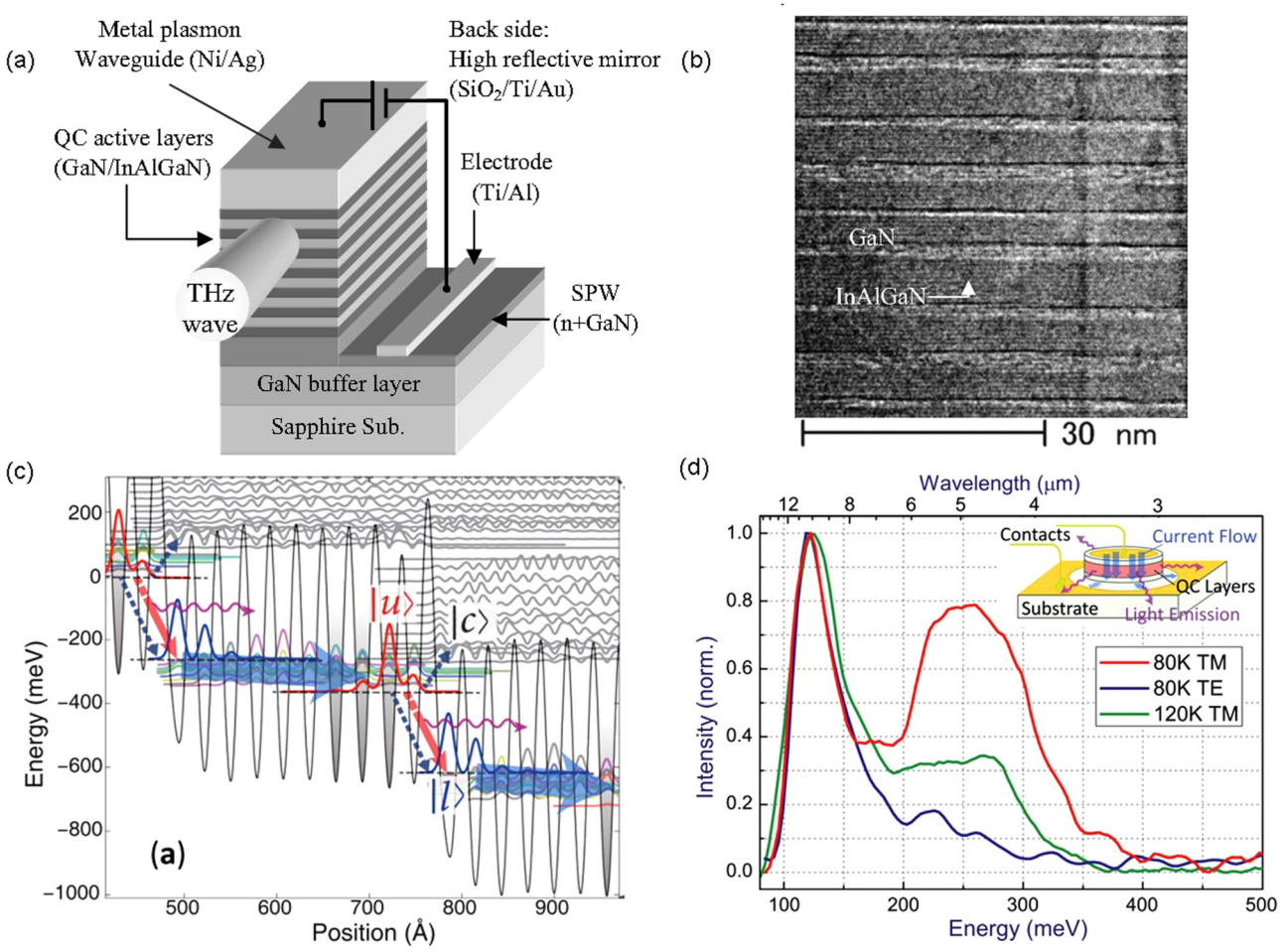

FIG. 14. (a) Schematic of AlInGaN/GaN THz QCL. (b) HR-TEM image of QC structures.[88] (c) CB of the III-nitride QC structure. Blue arrows indicate the direction of carrier flow whereas red arrows represent 4.9 μm optical transition. Blue dotted arrows demonstrate non-radiative leakage paths. (d) Emission spectra of the QC emitter (inset: schematic of the mesa isolated QC structure).[92] (a) and (b) Reproduced with permission from Terashima and Hirayama, Phys. Status Solidi C **6**, S615 (2009). Copyright 2009 John Wiley and Sons. (c) and (d) Reproduced with permission from Song *et al.*, Appl. Phys. Lett. **107**, 132104 (2015). Copyright 2015 AIP Publishing LLC.

effective interface grading that induces a continuous transition between QWs and barriers.

C. All-optical switches

Suzuki and Iizuka[16,26] and Iizuka *et al.*[28] demonstrated extremely short ISB absorption recovery time on the order of 140–400 ps, which is due to efficient electron LO phonon scattering in III-nitrides. All-optical switch is a device based on the fast recovery of ISBT process. When a signal at a suitable wavelength interacts with the all-optical switch, the signal is completely absorbed due to the ISB absorption. However, another control pulse can be used to saturate the ISB absorption, preventing the absorption of the signal pulse. Hence, the absorption of the signal depends on the presence or absence of the control pulse. Ultrafast all-optical switches could be the building block of ultrafast, all-optical networks. Iizuka *et al.*[93] achieved sub-picosecond modulation by ISBT in ridge waveguide with AlN/GaN QWs. A signal of 1.55 μm wavelength was modulated by 1.7 μm control wavelength with an ultrafast response of 0.36 ps. However, the control pulse energy of 120 pJ was too high for practical applications. Later, several all-optical switches were reported with reduced control pulse energy.[94–96] In 2009, Iizuka *et al.*[97] proposed methods to reduce the control pulse energy to 25 pJ, including decreasing the waveguide cross section and using tapered waveguides. In addition, it is also possible to reduce the control pulse using AlGaN/GaN QDs due to the higher density of QD and efficient ISBT process, where optical switching on the order of ~160 fs was achieved.[98] In short summary, all-optical switches with higher efficiency and small control pulse energies can be achieved using III-nitrides.

D. Electro-optical modulators

Electro-optical modulators are one of the key components in fiber-optical communication at the wavelength of 1.55 μm. It is predicted that III-nitrides based ISB modulators are capable of higher

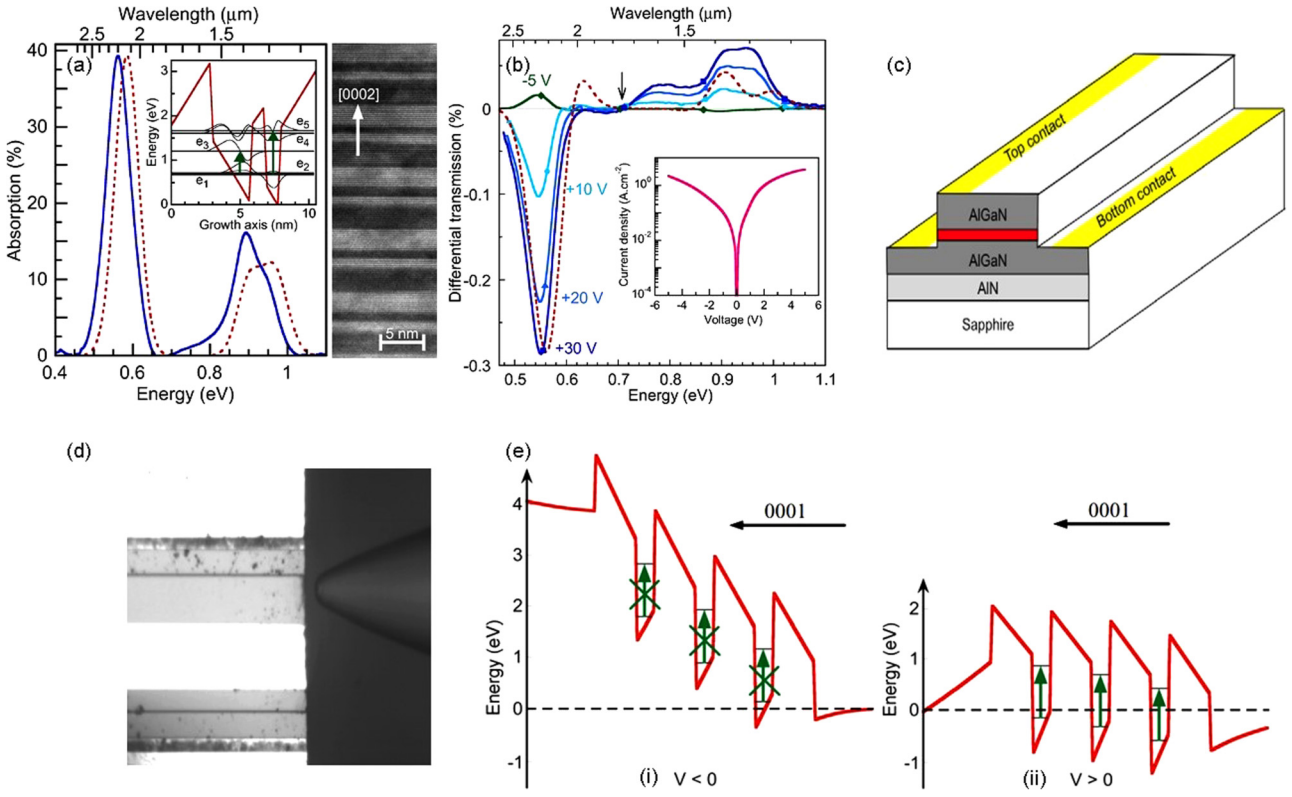

FIG. 15. (a) Room-temperature absorption spectrum for *p*-polarized light (solid curve) and calculated ISB absorption (dashed curve). Inset: CB profile and energy levels for one period of CQWs (left). HR-TEM image showing five periods of CQWs in the active region (right). (b) Differential transmission $\Delta T/T$ for applied bias pulses of +30 (squares), +20 (triangles), +10 (circles), and −5 V (diamonds). The dashed line shows the calculated transmission change for 0.8 V bias across the active region. Inset: Current density characteristic with applied voltage at room-temperature.[99] (c) Schematics of the depletion waveguide modulator. (d) Microscope image of one waveguide device with the lensed optical fiber used for light injection. The white regions are the metallic contacts. (e) The working principle of the depletion modulator. Under (i) negative applied bias, the QWs are depleted, and no absorption takes place, while under (ii) positive applied bias, the electron population of the wells gives rise to ISB absorption at 1.5 μm wavelength.[11] (a) and (b) Reproduced with permission from Nevou *et al.*, Appl. Phys. Lett. **90**, 223511 (2007). Copyright 2007 AIP Publishing LLC. (c)–(e) Reproduced with permission from New J. Phys. **11**, 125023 (2009). Copyright 2009 IOP Publishing.

bandwidth limits with low driving voltages.[10] Currently, there are only few reports of III-nitride ISB based electro-optical modulators. Nevou *et al.*[99] demonstrated short wavelength ISB electro-absorption modulation based on electron tunneling between AlN/GaN coupled QWs (CQWs). The active region of the structure consists of 3 nm GaN QW, 1 nm AlN coupling barrier, and another 1 nm GaN QW [the inset of Fig. 15(a)]. The thick GaN QW acts as the reservoir for 2.2 μm ISB absorption, while the 1 nm QW acts as the active QW for 1.3 μm ISB absorption. Figure 15(a) represents the absorption spectrum of *p*-polarized light with simulated curve. Two peaks were observed at 2.2 and 1.4 μm, where the 2.2 μm peak originated from e_1 to e_3 ISBTs. Moreover, 1.4 μm peak arises from e_2 and e_4 and e_2 and e_5 ISBTs with a small contribution from e_1 and e_5. When the device is positively biased, the electrons are transported from the reservoir to the active well with electro-absorption modulation at 1.2–1.67 μm. Figure 15(b) shows the differential transmission ($\Delta T/T$) under positive and negative biases. When it is reverse biased, the electrons are back transported to the reservoir, rendering the device transparent for absorbing wavelengths. Machandani *et al.*[11] showed 50 μm wide ridge waveguide ISB absorption-modulator that can be coupled with fiber optics [Figs. 15(c) and 15(d)]. The AlN/GaN QWs on *c*-plane sapphire were designed to have an absorption peak at 1.55 μm. With positive bias, the devices absorbed 1.5 μm wavelength, while reverse bias will deplete QWs, and the device was transparent for 1.5 μm wavelength [Fig. 15(e)]. Furthermore, ISB based refractive index modulators and phase modulators were also demonstrated.[100–102]

E. Resonant tunneling diodes

RTDs are tunneling diodes that use electron transport through quantum mechanical tunneling. Grinyaev and Razzhuvalov[103] theorized double-barrier resonant tunneling through AlGaN/GaN heterostructures. Sakr *et al.*[104] demonstrated resonant vertical electron transport through AlN/GaN QWs, whose conduction band diagram is shown in Fig. 16(a). Only the first QW is populated due

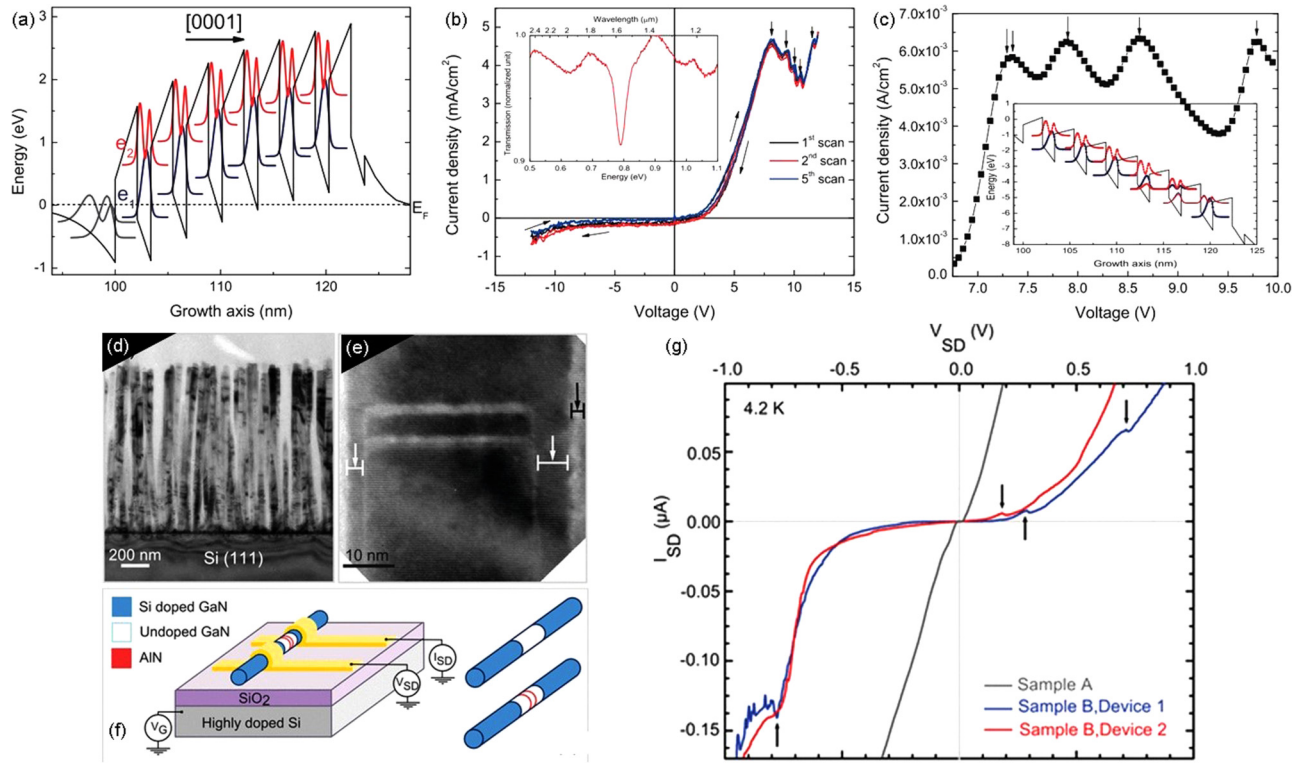

FIG. 16. (a) CB diagram of the AlN/GaN MQW structure under zero bias. (b) Room-temperature *J*–*V* characteristics, taken by applying a voltage cycle. The vertical arrows point to the NDRs. Inset: Measured IR transmission spectrum of the AlN/GaN MQW structure for TM-polarized light. (c) Theoretical *J*–*V* curve showing a series of NDRs due to the resonant tunneling between the e_1 and e_2' states of adjacent QWs. Inset: CB diagram at 7.1 V that shows the strong coupling between the e_1 and e_2' states of adjacent QWs.[104] (d) TEM image of GaN NWs grown on a Si(111) substrate. (e) HR-TEM image a NW section containing a double-barrier heterostructure, i.e., a pair 2 nm thick AlN barriers (bright contrast) separated by a 6 nm height GaN quantum dot. (f) Schematic of a single NW based device with metal contacts on an oxidized Si substrate (left). The top (bottom) right scheme shows an n–i–n NW without (with) AlN double tunnel barriers. (g) I_{SD}–V_{SD} characteristics at 4.2 K of GaN NWs with two closely spaced AlN tunnel barriers in comparison to that of n–i–n GaN NWs.[105] (a)–(c) Reproduced with permission from Sakr *et al.*, Appl. Phys. Express **5**, 052203 (2012). Copyright 2012 IOP Publishing. (d)–(g) Reproduced with permission from Songmuang *et al.*, Nano Lett. **10**, 3545 (2010). Copyright 2010 American Chemical Society.

to the fact that it is below the Fermi level. ISB transmission showed a dip at 1.57 μm due to the ISB absorption of QWs. In Fig. 16(b), five negative differential resistance (NDR) features were observed due to the electron transport. The main NDR feature corresponded to the alignment of the ground states of QWs, while other residual features were due to the alignment between excited and fundamental states of adjacent QWs. This NDR features were in good agreement with theoretical simulation in Fig. 16(c). Songmuang *et al.*[105] showed quantum electron transport through AlN/GaN double-barrier heterostructure NWs [Figs. 16(d)–16(f)]. Figure 16(g) shows the NDR features at both positive and negative bias for GaN NWs with AlN barriers. NWs showed lower resonant tunneling voltage compared to QWs [Fig. 16(b)]. It is evident that observed tunneling came from the AlN barriers in NWs as opposed to the undoped n–i–n sample in QWs [Fig. 16(g)]. Rigutti *et al.*[106] observed electron transport through AlN/GaN NDs in GaN NWs. Two structures were fabricated such that AlN/GaN NDs are covered with and without GaN shell. They found that NDs with GaN shell did not necessarily show NDR due to the electron transport mainly in the GaN shell not through NDs. The electron transport is restricted to a narrow surface region of the GaN shell. However, the structure that has NDs without GaN shell, actively participated in the quantum transport of electrons to exhibit NDR features.

VI. CONCLUSION AND OUTLOOK

III-nitrides based ISBT has gained considerable momentum due to tunable spectral response from near-IR to THz and promising room-temperature operation because of large LO phonon energy. This paper comprehensively reviews the recent progress of nonpolar and semipolar III-nitrides based ISBT from the aspects of materials, structures, devices, and applications. Nonpolar and semipolar III-nitrides have eliminated or reduced spontaneous and piezoelectric polarization effects compared with polar *c*-plane III-nitride. This leads to the flatband profile and large wavefunction overlap with improved ISBT efficiency and frequency range. Furthermore, nonpolar and semipolar III-nitride ISBT showed excellent wavelength tunability by active region width, barrier width, barrier alloy content, and doping. Furthermore, several structures have been demonstrated for III-nitride ISBT, including QWs, QDs, NWs, and cubic III-nitrides. Among them, AlGaN/GaN QWs are the most popular ISBT structure. The effects of polarizations and doping on the ISBT properties of AlGaN/GaN QWs have been theoretically and experimentally studied. It was found that semipolar planes with inclination angle larger than 55° are optimal for long wavelength and THz applications with high efficiency, and modulation doping in the barrier such as δ-doping could also enhance the ISBT performance. However, experimental demonstration of nonpolar and semipolar III-nitrides ISBT is still scarce due to the challenges in growing high-quality epitaxial heterostructures with abrupt interfaces. Furthermore, the reported devices still need to be measured under cryogenic temperatures, and room-temperature operation is still elusive at THz spectral regime. Despite these challenges, III-nitrides based ISBT have been employed in some devices and applications with great performance compared with the state-of-the-art AlGaAs/GaAs based ISBT devices, including photodetectors (QWIPs and QCDs), QCLs, RTDs, electro-optical modulators, and all-optical switches.

In addition to III-nitride materials, future development of ISBT based systems can also search for material systems with high conduction band offsets to achieve a wide accessible wavelength range. Improvements in epitaxial growth techniques will be needed to precisely engineer atomic-layer thickness with low interface roughness, leading to higher transition strengths with lower scattering rates. High conduction band offset material systems can enable near-IR ISBT capability for optical communications to take advantage of the low-loss transmission window of fiber optics. Due to high optical non-linearities and ultrafast relaxation times, AlGaN/GaN systems are suitable for all-optical switches with bit rates larger than 100 Gbs^{-1}, which will play a leading role in the future ultra-broadband all-optical networks for information transmission and processing in the optical domain. On the other hand, ISBT in longer wavelengths requires reduced polarization-induced electric fields using nonpolar and semipolar III-nitrides, which poses challenges in material growth. Room-temperature solid-state THz devices will gain significant momentum in the coming years, where III-nitride ISBT can be a gamechanger. THz spectroscopy in condensed matter physics is an exciting new field of study where meV energy radiation can be used to excite charge carriers, quasiparticles, and polaritons in semiconductors, semi-metals, superconductors, and topological insulators where new physics can be investigated. This field can be significantly advanced by compact semiconductor based THz emitters and detectors, where the current system is bulky, expensive, and less power efficient. Furthermore, on-chip THz-sensors can be used as biological sensors. Another interesting direction of ISBT is "artificial atoms," where ISBT can be designed to imitate optical transitions in an atomic system. More interestingly, several artificial atoms can be coupled to form artificial molecules with new physics and phenomena. Finally, with solid-state THz optoelectronic devices with small fingerprints, it is possible to realize photonic integrated circuits using III-nitride ISBT components. With the improvement of epitaxial techniques, new QW, QD, and NW structural designs will come into play to achieve higher efficiencies and gains. With the advancement of epitaxial growth techniques and device design, new pathways for nonlinear optics, quantum optics, light–matter interaction, and phonon engineering will emerge through III-nitride ISBT, and high-performance room-temperature nonpolar and semipolar III-nitrides based ISBT holds great potential for applications in sensing, biomedical imaging, communication, photonic device integration and ultrafast optoelectronics.

ACKNOWLEDGMENTS

This work was partially supported by the Iowa State University Regents Innovation Fund, the grant from Army Research Office (ARO) PECASE (Grant No. W911NF-19-1-0089), and as part of ULTRA, an Energy Frontier Research Center funded by the U.S. Department of Energy, Office of Science, Basic Energy Sciences under Award No. DE-SC0021230.

AUTHOR DECLARATIONS

Conflict of Interest

The authors have no conflicts to disclose.

DATA AVAILABILITY

The data that support the results and conclusions of this study are available within the article.

REFERENCES

[1]H. Fu, K. Fu, S. Chowdhury, T. Palacios, and Y. Zhao, "Vertical GaN power devices: Device principles and fabrication technologies—Part I," IEEE Trans. Electron Devices **68**, 3200 (2021).

[2]H. Fu, K. Fu, S. Chowdhury, T. Palacios, and Y. Zhao, "Vertical GaN power devices: Device principles and fabrication technologies—Part II," IEEE Trans. Electron Devices **68**, 3212 (2021).

[3]Y. Zhang, A. Zubair, Z. Liu, M. Xiao, J. Perozek, Y. Ma, and T. Palacios, "Gan FinFETs and trigate devices for power and RF applications: Review and perspective," Semicond. Sci. Technol. **36**, 054001 (2021).

[4]Y. Zhao, H. Fu, G. T. Wang, and S. Nakamura, "Toward ultimate efficiency: Progress and prospects on planar and 3D nanostructured nonpolar and semipolar InGaN light-emitting diodes," Adv. Opt. Photonics **10**, 246 (2018).

[5]Y. Zhao, S.-H. Oh, F. Wu, Y. Kawaguchi, S. Tanaka, K. Fujito, J. S. Speck, S. P. DenBaars, and S. Nakamura, "Green semipolar (20-2-1) InGaN light-emitting diodes with small wavelength shift and narrow spectral linewidth," Appl. Phys. Express **06**, 062102 (2013).

[6]H. Fu and Y. Zhao, "Efficiency droop in InGaN/GaN LEDs," in *Nitride Semiconductor Light-Emitting Diodes (LEDs): Materials, Technologies, and Applications*, 2nd ed., edited by J. J. Huang, H. C. Kuo, and S. C. Shen (Woodhead publishing, 2018).

[7]Y. Zhao, J. Sonada, I. Koslow, C.-C. Pan, H. Ohta, J.-S. Ha, S. P. DenBaars, and S. Nakamura, "Optimization of device structures for bright blue semipolar (1011) light emitting diodes via metalorganic chemical vapor deposition," Jpn. J. Appl. Phys. **49**, 070206 (2010).

[8]D. Hofstetter, S. Schad, H. Wu, W. Schaff, and L. Eastman, "GaN/AlN-based quantum-well infrared photodetector for 1.55 μm," Appl. Phys. Lett. **83**, 572 (2003).

[9]M. Beeler, E. Trichas, and E. Monroy, "III-nitride semiconductors for intersubband optoelectronics: A review," Semicond. Sci. Technol. **28**, 074022 (2013).

[10]B. Gil, *III-Nitride Semiconductors and Their Modern Devices* (Oxford University Press, Oxford, 2013).

[11]H. Machhadani, P. Kandaswamy, S. Sakr, A. Vardi, A. Wirtmüller, L. Nevou, F. Guillot, G. Pozzovivo, M. Tchernycheva, A. Lupu, L. Vivien, P. Crozat, E. Warde, C. Bougerol, S. Schacham, G. Strasser, G. Bahir, E. Monroy, and F. H. Julien, "GaN/AlGaN intersubband optoelectronic devices," New J. Phys. **11**, 125023 (2009).

[12]E. Tournié and L. Cerutti, *Mid-infrared Optoelectronics Materials, Devices, and Applications* (Woodhead Publishing, 2019).

[13]E. Bellotti, K. Driscoll, T. Moustakas, and R. Paiella, "Monte Carlo study of GaN vs GaAs terahertz quantum cascade structures," Appl. Phys. Lett. **92**, 101112 (2008).

[14]A. Kamgar, P. Kneschaurek, G. Dorda, and J. Koch, "Resonance spectroscopy of electronic levels in a surface accumulation layer," Phys. Rev. Lett. **32**, 1251 (1974).

[15]L. C. West and S. J. Eglash, "First observation of an extremely large-dipole infrared transition within the conduction band of a GaAs quantum well," Appl. Phys. Lett. **46**, 1156 (1985).

[16]N. Suzuki and N. Iizuka, "Feasibility study on ultrafast nonlinear optical properties of 1.55-μm intersubband transition in AlGaN/GaN quantum wells," Jpn. J. Appl. Phys. **36**, L1006 (1997).

[17]K. Sink, G. Bahir, A. Abare, S. DenBaars, and J. Bowers, in Technical Digest of the 1997 Electronic Materials Conference, Fort Collins, CO, *25–27 June 1997*.

[18]M. M. Hussain, *Advanced Nanoelectronics: Post-Silicon Materials and Devices* (John Wiley and Sons, 2019).

[19]A. M. Andrews, T. Zederbauer, H. Detz, D. MacFarland, W. Schrenk, and G. Strasser, "Chapter 26—THz quantum cascade lasers," in *Molecular Beam Epitaxy*, 2nd ed., edited by Mohamed Henini (Elsevier, 2018).

[20]C. Wood and D. Jena, *Polarization Effects in Semiconductors: From AB Initio Theory to Device Applications* (Springer Science Business Media LLC, Boston, 2008).

[21]Y. Zhao, H. Fu, G. T. Wang, and S. Nakamura, "Toward ultimate efficiency: Progress and prospects on planar and 3D nanostructured nonpolar and semipolar InGaN light-emitting diodes," Adv. Opt. Photonics **10**, 246 (2018).

[22]H. Fu, Z. Lu, X. Huang, H. Chen, and Y. Zhao, "Crystal orientation dependent intersubband transition in semipolar AlGaN/GaN single quantum well for optoelectronic applications," J. Appl. Phys. **119**, 174502 (2016).

[23]R. M. Farrell, E. C. Yong, F. Wu, S. P. DenBaars, and J. S. Speck, "Materials and growth issues for high-performance nonpolar and semipolar light-emitting devices," Semicond. Sci. Technol. **27**, 024001 (2012).

[24]M. Helm, "Chapter 1: The basic physics of intersubband transitions," in *Semiconductors and Semimetals*, edited by F. Capasso and H. C. Liu (Elsevier, 1999), Vol. 62.

[25]K. Hoshino, T. Someya, K. Hirakawa, and Y. Arakawa, "Observation of intersubband transition from the first to the third subband (e1–e3) in GaN/AlGaN quantum wells," Phys. Status Solidi A **192**, 27 (2002).

[26]N. Suzuki and N. Iizuka, "Electron scattering rates in AlGaN/GaN quantum wells for 1.55-μm inter-subband transition," Jpn. J. Appl. Phys. **37**, L369 (1998).

[27]N. Suzuki and N. Iizuka, "Effect of polarization field on intersubband transition in AlGaN/GaN quantum wells," Jpn. J. Appl. Phys. **38**, L363 (1999).

[28]N. Iizuka, K. Kaneko, N. Suzuki, T. Asano, S. Noda, and O. Wada, "Ultrafast intersubband relaxation (<150 fs) in AlGaN/GaN multiple quantum wells," Appl. Phys. Lett. **77**, 648 (2000).

[29]C. Gmachl, H. Ng, S. G. Chu, and A. Cho, "Intersubband absorption at $\lambda \sim 1.55\,\mu$m in well- and modulation-doped GaN/AlGaN multiple quantum wells with superlattice barriers," Appl. Phys. Lett. **77**, 3722 (2000).

[30]C. Gmachl, S. Frolov, H. Ng, S. Chu, and A. Cho, "Sub-picosecond electron scattering time for $\lambda \simeq 1.55\,\mu$m intersubband transitions in GaN/AlGaN multiple quantum wells," Electron. Lett. **37**, 378 (2001).

[31]C. Gmachl, H. Ng, and A. Cho, "Intersubband absorption in degenerately doped GaN/AlGaN coupled double quantum wells," Appl. Phys. Lett. **79**, 1590 (2001).

[32]J. Heber, C. Gmachl, H. Ng, and A. Cho, "Comparative study of ultrafast intersubband electron scattering times at 1.55 μm wavelength in GaN/AlGaN heterostructures," Appl. Phys. Lett. **81**, 1237 (2002).

[33]H. Ng, C. Gmachl, J. Heber, J. Hsu, S. Chu, and A. Cho, "Recent progress in GaN-based superlattices for near-infrared intersubband transitions," Phys. Status Solidi B **234**, 817 (2002).

[34]N. Péré-Laperne, C. Bayram, L. Nguyen-Thê, R. McClintock, and M. Razeghi, "Tunability of intersubband absorption from 4.5 to 5.3 μm in a GaN/AlGaN superlattices grown by metal-organic chemical vapor deposition," Appl. Phys. Lett. **95**, 131109 (2009).

[35]P. K. Kandaswamy, H. Machhadani, C. Bougerol, S. Sakr, M. Tchernycheva, F. H. Julien, and E. Monroy, "Midinfrared intersubband absorption in GaN/AlGaN superlattices on Si(111) templates," Appl. Phys. Lett. **95**, 141911 (2009).

[36]P. K. Kandaswamy, H. Machhadani, Y. Kotsar, S. Sakr, A. Das, M. Tchernycheva, L. Rapenne, E. Sarigiannidou, F. H. Julien, and E. Monroy, "Effect of doping on the mid-infrared intersubband absorption in GaN/AlGaN superlattices grown on Si(111) templates," Appl. Phys. Lett. **96**, 141903 (2010).

[37]H. Machhadani, Y. Kotsar, S. Sakr, M. Tchernycheva, R. Colombelli, J. Mangeney, E. Bellet-Amalric, E. Sarigiannidou, E. Monroy, and F. H. Julien, "Terahertz intersubband absorption in GaN/AlGaN step quantum wells," Appl. Phys. Lett. **97**, 191101 (2010).

[38]P. K. Kandaswamy, F. Guillot, E. Bellet-Amalric, E. Monroy, L. Nevou, M. Tchernycheva, A. Michon, F. H. Julien, E. Baumann, F. R. Giorgetta, D. Hofstetter, T. Remmele, M. Albrecht, S. Birner, and L. S. Dang, "GaN/AlN short-period superlattices for intersubband optoelectronics: A systematic study of their epitaxial growth, design, and performance," J. Appl. Phys. **104**, 093501 (2008).
[39]J. Zhu, S.-L. Ban, and S.-H. Ha, "Phonon-assisted intersubband transitions in wurtzite GaN/InxGa$_{1-x}$N quantum wells," Chin. Phys. B **21**, 097301 (2012).
[40]G. Chen, X. Wang, X. Rong *et al.*, "Intersubband transition in GaN/InGaN multiple quantum wells," Sci. Rep. **5**, 11485 (2015).
[41]S. Nicolay, J.-F. Carlin, E. Feltin, R. Butte, M. Mosca, N. Grandjean, M. Ilegems, M. Tchernycheva, L. Nevou, and F. H. Julien, "Midinfrared intersubband absorption in lattice-matched AlInN/GaN multiple quantum wells," Appl. Phys. Lett. **87**, 111106 (2005).
[42]O. Malis, C. Edmunds, M. J. Manfra, and D. L. Sivco, "Near-infrared intersubband absorption in molecular-beam epitaxy-grown lattice-matched InAlN/GaN superlattices," Appl. Phys. Lett. **94**, 161111 (2009).
[43]G. Cywinski *et al.*, "Growth of thin AlInN/GaInN quantum wells for applications to high-speed intersubband devices at telecommunication wavelengths," J. Vac. Sci. Technol. B **24**, 1505 (2006).
[44]H. Akabli, A. Almaggoussi, A. Abounadi, A. Rajira, K. Berland, and T. G. Andersson, "Intersubband energies in Al$_{1-y}$In$_y$N/Ga$_{1-x}$In$_x$N heterostructures with lattice constant close to AGaN," Superlattices Microstruct. **52**, 70 (2012).
[45]H. Machhadani, M. Tchernycheva, S. Sakr, L. Rigutti, R. Colombelli, E. Warde, C. Mietze, D. J. As, and F. H. Julien, "Intersubband absorption of cubic GaN/Al(Ga)N quantum wells in the near-infrared to terahertz spectral range," Phys. Rev. B **83**, 075313 (2011).
[46]E. A. DeCuir, E. Fred, M. O. Manasreh, J. Schormann, D. J. As, and K. Lischka, "Near-infrared intersubband absorption in nonpolar cubic GaN/AlN superlattices," Appl. Phys. Lett. **91**, 041911 (2007).
[47]E. A. DeCuir, M. O. Manasreh, E. Tschumak, J. Schormann, D. J. As, and K. Lischka, "Cubic GaN/AlN multiple quantum well photodetector," Appl. Phys. Lett. **92**, 201910 (2008).
[48]M. Tchernycheva, L. Nevou, L. Doyennette, F. H. Julien, E. Warde, F. Guillot, E. Monroy, E. Bellet-Amalric, T. Remmele, and M. Albrecht, "Systematic experimental and theoretical investigation of intersubband absorption in GaN/AlN quantum wells," Phys. Rev. B **73**, 125347 (2006).
[49]K. Moumanis, A. Helman, F. Fossard, M. Tchernycheva, A. Lusson, F. Julien, B. Damilano, N. Grandjean, and J. Massies, "Intraband absorptions in GaN/AlN quantum dots in the wavelength range of 1.27–2.4 μm," Appl. Phys. Lett. **82**, 868 (2003).
[50]V. Chamard, T. Schulli, M. Sztucki, T. Metzger, E. Sarigiannidou, J. Rouviere, M. Tolan, C. Adelmann, and B. Daudin, "Strain distribution in nitride quantum dot multilayers," Phys. Rev. B **69**, 125327 (2004).
[51]M. Tchernycheva, L. Nevou, L. Doyennette, A. Helman, R. Colombelli, F. Julien, F. Guillot, E. Monroy, T. Shibata, and M. Tanaka, "Intraband absorption of doped GaN/AlN quantum dots at telecommunication wavelengths," Appl. Phys. Lett. **87**, 101912 (2005).
[52]S. Tamariz, G. Callsen, and N. Grandjean, "Density control of GaN quantum dots on AlN single crystal," Appl. Phys. Lett. **114**, 082101 (2019).
[53]M. Beeler, P. Hille, J. Schörmann, J. Teubert, M. de la Mata, J. Arbiol, M. Eickhoff, and E. Monroy, "Intraband absorption in self-assembled Ge-doped GaN/AlN nanowire heterostructures," Nano Lett. **14**, 1665 (2014).
[54]A. Ajay, R. Blasco, J. Polaczyński, M. Spies, M. I. Den Hertog, and E. Monroy, "Intersubband absorption in GaN nanowire heterostructures at mid-infrared wavelengths," Nanotechnology **29**, 385201 (2018).
[55]H. Fu, H. Chen, X. Huang, Z. Lu, and Y. Zhao, "Theoretical analysis of modulation doping effects on intersubband transition properties of semipolar AlGaN/GaN quantum well," J. Appl Phys. **121**, 014501 (2017).
[56]M. Monavarian, J. Xu, M. N. Fireman, N. Nookala, F. Wu, B. Bonef, K. S. Qwah, E. C. Young, M. A. Belkin, and J. S. Speck, "Structural and optical properties of nonpolar *m*- and *a*-plane GaN/AlGaN heterostructures for narrow-linewidth mid-infrared intersubband transitions," Appl. Phys. Lett. **116**, 201103 (2020).
[57]C. B. Lim, M. Beeler, A. Ajay, J. Lähnemann, E. Bellet-Amalric, C. Bougerol, and E. Monroy, "Intersubband transitions in nonpolar GaN/Al(Ga)N heterostructures in the short- and mid-wavelength infrared regions," J. Appl. Phys. **118**, 014309 (2015).
[58]A. Pesach, E. Gross, C.-Y. Huang, Y.-D. Lin, A. Vardi, S. E. Schacham, S. Nakamura, and G. Bahir, "Non-polar *m*-plane intersubband based InGaN/(Al)GaN quantum well infrared photodetectors," Appl. Phys. Lett. **103**, 022110 (2013).
[59]C. B. Lim, M. Beeler, A. Ajay, J. Lähnemann, E. Bellet-Amalric, C. Bougerol, J. Schörmann, M. Eickhoff, and E. Monroy, "Short-wavelength, mid- and far-infrared intersubband absorption in nonpolar GaN/Al(Ga)N heterostructures," Jpn. J. Appl. Phys. **55**, 05FG05 (2016).
[60]C. B. Lim, A. Ajay, C. Bougerol, J. Lähnemann, F. Donatini, J. Schörmann, E. Bellet-Amalric, D. A. Browne, M. Jiménez-Rodríguez, and E. Monroy, "Effect of doping on the far-infrared intersubband transitions in nonpolar m-plane GaN/AlGaN heterostructures," Nanotechnology **27**, 145201 (2016).
[61]T. Nguyen, B. Dzuba, Y. Cao, A. Senichev, R. E. Diaz, M. J. Manfra, and O. Malis, "Mid-infrared intersubband absorption in strain-balanced nonpolar (In)AlGaN/InGaN multi-quantum wells," Opt. Mater. Express **11**, 3284 (2021).
[62]H. Machhadani, M. Beeler, S. Sakr, E. Warde, Y. Kotsar, M. Tchernycheva, M. P. Chauvat, P. Ruterana, G. Nataf, P. De Mierry, E. Monroy, and F. H. Julien, "Systematic study of near-infrared intersubband absorption of polar and semipolar GaN/AlN quantum wells," J. Appl. Phys. **113**, 143109 (2013).
[63]L. Lahourcade, P. K. Kandaswamy, J. Renard, P. Ruterana, H. Machhadani, M. Tchernycheva, F. H. Julien, B. Gayral, and E. Monroy, "Interband and intersubband optical characterization of semipolar (11–22)-oriented GaN/AlN multiple-quantum-well structures," Appl. Phys. Lett. **93**, 111906 (2008).
[64]F. Sudradjat, W. Zhang, J. Woodward, H. Durmaz, T. Moustakas, and R. Paiella. "Far-infrared intersubband photodetectors based on double-step Ill-nitride quantum wells," Appl. Phys. Lett. **100**, 241113 (2012).
[65]E. Baumann, F. Giorgetta, D. Hofstetter, H. Lu, X. Chen, W. Schaff, L. Eastman, S. Golka, W. Schrenk, and G. Strasser, "Intersubband photoconductivity at 1.6 μm using a strain-compensated AlN/ GaN superlattice," Appl. Phys. Lett. **87**, 191102 (2005).
[66]H. Uchida, S. Matsui, P. Holmstrom, A. Kikuchi, and K. Kishino, "Room-temperature operation of 1.55 μm wavelength-range GaN/AlN quantum well intersubband photodetectors," IEICE Electron. Exp. **2**, 566 (2005).
[67]D. Hofstetter, E. Baumann, F. Giorgetta, M. Graf, M. Maier, F. Guillot, E. Bellet-Amalric, and E. Monroy, "High-quality AlN/GaN-superlattice structures for the fabrication of narrow-band 1.4 μm photovoltaic intersubband detectors," Appl. Phys. Lett. **88**, 121112 (2006).
[68]E. Baumann, F. Giorgetta, D. Hofstetter, S. Golka, W. Schrenk, G. Strasser, L. Kirste, S. Nicolay, E. Feltin, J. Carlin *et al.*, "Near infrared absorption and room temperature photovoltaic response in AlN/GaN superlattices grown by metal-organic vapor-phase epitaxy," Appl. Phys. Lett. **89**, 041106 (2006).
[69]H. Durmaz, D. Nothern, G. Brummer, T. D. Moustakas, and R. Paiella, "Terahertz intersubband photodetectors based on semi-polar GaN/AlGaN heterostructures," Appl. Phys. Lett. **108**, 201102 (2016).
[70]D. Hofstetter, J. Di Francesco, P. Kandaswamy, A. Das, S. Valdueza- Felip, and E. Monroy, "Performance improvement of AlN-GaN-based intersubband detectors by using quantum dots," IEEE Photonics Technol. Lett. **22**, 1087 (2010).
[71]L. Doyennette, L. Nevou, M. Tchernycheva, A. Lupu, F. Guillot, E. Monroy, R. Colombelli, and F. Julien, "GaN-based quantum dot infrared photodetector operating at 1.38 μm," Electron. Lett. **41**, 1077 (2005).
[72]L. Doyennette, A. Vardi, F. Guillot, L. Nevou, M. Tchernycheva, A. Lupu, R. Colombelli, G. Bahir, E. Monroy, and F. Julien, "Intraband photodetection at 1.3–1.5 μm in self-organized GaN/AlN quantum dots," Phys. Status Solidi B **243**, 3993 (2006).
[73]A. Vardi, N. Akopian, G. Bahir, L. Doyennette, M. Tchernycheva, L. Nevou, F. Julien, F. Guillot, and E. Monroy, "Room-temperature demonstration of GaN/

AlN quantum dot intraband infrared photodetector at fiber-optics communication wavelength," Appl. Phys. Lett. **88**, 143101 (2006).
[74]A. Vardi, G. Bahir, F. Guillot, C. Bougerol, E. Monroy, S. Schacham, M. Tchernycheva, and F. Julien, "Near-infrared quantum cascade detector in GaN/AlGaN/AlN heterostructures," Appl. Phys. Lett. **92**, 011112 (2008).
[75]A. Vardi, N. Kheirodin, L. Nevou, H. Machhadani, L. Vivien, P. Crozat, M. Tchernycheva, R. Colombelli, F. Julien, F. Guillot *et al.*, "High-speed operation of GaN/AlGaN quantum cascade detectors at $\lambda \sim 1.55\,\mu$m," Appl. Phys. Lett. **93**, 193509 (2008).
[76]Y. Song, R. Bhat, T.-Y. Huang, P. Badami, C.-E. Zah, and C. Gmachl, "III-nitride quantum cascade detector grown by metal organic chemical vapor deposition," Appl. Phys. Lett. **105**, 182104 (2014).
[77]S. Sakr, E. Giraud, M. Tchernycheva, N. Isac, P. Quach, E. Warde, N. Grandjean, and F. Julien, "A simplified GaN/AlGaN quantum cascade detector with an alloy extractor," Appl. Phys. Lett. **101**, 251101 (2012).
[78]S. Sakr, E. Giraud, A. Dussaigne, M. Tchernycheva, N. Grandjean, and F. Julien, "Two-color GaN/AlGaN quantum cascade detector at short infrared wavelengths of 1 and 1.7 μm," Appl. Phys. Lett. **100**, 181103 (2012).
[79]S. Sakr, P. Crozat, D. Gacemi, Y. Kotsar, A. Pesach, P. Quach, N. Isac, M. Tchernycheva, L. Vivien, G. Bahir, E. Monroy, and F. H. Julien, "Gan/AlGaN waveguide quantum cascade photodetectors at $\lambda \approx 1.55\,\mu$m with enhanced responsivity and ~40 GHz frequency bandwidth," Appl. Phys. Lett. **102**, 011135 (2013).
[80]R. Köhler, A. Tredicucci, F. Beltram *et al.*, "Terahertz semiconductor-heterostructure laser," Nature **417**, 156 (2002).
[81]L. Bosco, M. Franckié, G. Scalari, M. Beck, A. Wacker, and J. Faist, "Thermoelectrically cooled THz quantum cascade laser operating up to 210 K," Appl. Phys. Lett. **115**, 010601 (2019).
[82]A. Khalatpour, A. K. Paulsen, C. Deimert, Z. R. Wasilewski, and Q. Hu, "High-power portable terahertz laser systems," Nat. Photonics **15**, 16 (2021).
[83]H. Hirayama and W. Terashima, "Recent progress toward realizing GaN-based THz quantum cascade laser," in Proc. SPIE **8993**, 89930G (2014).
[84]B. S. Williams, H. Callebaut, S. Kumar, Q. Hu, and J. L. Reno, "3.4-THz quantum cascade laser based on longitudinal-optical-phonon scattering for depopulation," Appl. Phys. Lett. **82**, 1015 (2003).
[85]J. T. Lu and J. C. Cao, "Monte Carlo simulation of hot phonon effects in resonant-phonon-assisted terahertz quantum-cascade lasers," Appl. Phys. Lett. **88**, 061119 (2006).
[86]V. D. Jovanovic, D. Indjin, Z. Ikonic, and P. Harrison, "Simulation and design of GaN/AlGaN far-infrared ($\lambda \sim 34\,\mu$m) quantum-cascade laser," Appl. Phys. Lett. **84**, 2995 (2004).
[87]G. Sun, R. A. Soref, and J. B. Khurgin, "Active region design of a terahertz GaN/$Al_{0.15}Ga_{0.85}N$ quantum cascade laser," Superlattices Microstruct. **37**, 107 (2005).
[88]W. Terashima and H. Hirayama, "Design and fabrication of terahertz quantum cascade laser structure based on III-nitride semiconductors," Phys. Status Solidi C **6**, S615 (2009).
[89]W. Terashima and H. Hirayama, "The utility of droplet elimination by thermal annealing technique for fabrication of GaN/AlGaN terahertz quantum cascade structure by radio frequency molecular beam epitaxy," Appl. Phys. Express **3**, 125501 (2010).
[90]W. Terashima and H. Hirayama, "Spontaneous emission from GaN/AlGaN terahertz quantum cascade laser grown on GaN substrate," Phys. Status Solidi C **8**, 2302 (2011).
[91]W. Terashima and H. Hirayama, "Terahertz intersubband electroluminescence from GaN/AlGaN quantum cascade laser structure on AlGaN template," in *2011 International Conference on Infrared, Millimeter, and Terahertz Waves* (IEEE, 2011), pp. 1–2.
[92]A. Y. Song, R. Bhat, A. A. Allerman, J. Wang, T.-Y. Huang, C.-E. Zah, and C. F. Gmachl, "Quantum cascade emission in the III-nitride material system designed with effective interface grading," Appl. Phys. Lett. **107**, 132104 (2015).
[93]N. Iizuka, K. Kaneko, and N. Suzuki, "Sub-picosecond modulation by intersubband transition in ridge waveguide with GaN/AlN quantum wells," Electron. Lett. **40**, 962 (2004).
[94]N. Iizuka, K. Kaneko, and N. Suzuki, "Sub-picosecond all-optical gate utilizing an intersubband transition," Opt. Express **13**, 3835 (2005).
[95]N. Iizuka, K. Kaneko, and N. Suzuki, "All-optical switch utilizing intersubband transition in GaN quantum wells," IEEE J. Quantum Electron. **42**, 765 (2006).
[96]N. Iizuka, K. Kaneko, and N. Suzuki, "Polarization dependent loss in III-nitride optical waveguides for telecommunication devices," J. Appl. Phys. **99**, 093107 (2006).
[97]N. Iizuka, H. Yoshida, N. Managaki, T. Shimizu, S. Hassanet, C. Cumtornkittikul, M. Sugiyama, and Y. Nakano, "Integration of GaN/AlN all-optical switch with SiN/AlN waveguide utilizing spot-size conversion," Opt. Express **17**, 23247 (2009).
[98]L. Nevou, J. Mangeney, M. Tchernycheva, F. Julien, F. Guillot, and E. Monroy, "Ultrafast relaxation and optical saturation of intraband absorption of GaN/AlN quantum dots," Appl. Phys. Lett. **94**, 132104 (2009).
[99]L. Nevou, N. Kheirodin, M. Tchernycheva, L. Meignien, P. Crozat, A. Lupu, E. Warde, F. Julien, G. Pozzovivo, S. Golka *et al.*, "Short-wavelength intersubband electroabsorption modulation based on electron tunneling between GaN/AlN coupled quantum wells," Appl. Phys. Lett. **90**, 223511 (2007).
[100]L. Cen, B. Shen, Z. Qin, and G. Zhang, "Influence of polarization induced electric fields on the wavelength and the refractive index of intersubband transitions in AlN/GaN coupled double quantum wells," J. Appl. Phys. **105**, 093109 (2009).
[101]Y. Li, A. Bhattacharyya, C. Thomidis, Y. Liao, T. Moustakas, and R. Paiella, "Refractive-index nonlinearities of intersubband transitions in GaN/AlN quantum-well waveguides," J. Appl. Phys. **104**, 083101 (2008).
[102]A. Lupu, M. Tchernycheva, Y. Kotsar, E. Monroy, and F. Julien, "Electroabsorption and refractive index modulation induced by intersubband transitions in GaN/AlN multiple quantum wells," Opt. Express **20**, 12541 (2012).
[103]S. N. Grinyaev and A. N. Razzhuvalov, "Resonant electron tunneling in GaN/$Ga_{1-x}Al_xN$ (0001) strained structures with spontaneous polarization and piezoeffect," Phys. Solid State **43**, 549 (2002).
[104]S. Sakr, Y. Kotsar, M. Tchernycheva, E. Warde, N. Isac, E. Monroy, and F. H. Julien, "Resonant tunneling transport in a GaN/AlN multiple-quantum-well structure," Appl. Phys. Express **5**, 052203 (2012).
[105]R. Songmuang, G. Katsaros, E. Monroy, P. Spathis, C. Bougerol, M. Mongillo, and S. De Franceschi, "Quantum transport in GaN/AlN double-barrier heterostructure nanowires," Nano Lett. **10**, 3545 (2010).
[106]L. Rigutti, G. Jacopin, A. D. L. Bugallo, M. Tchernycheva, E. Warde, F. H. Julien, R. Songmuang, E. Galopin, L. Largeau, and J.-C. Harmand, "Investigation of the electronic transport in GaN nanowires containing GaN/AlN quantum discs," Nanotechnology **21**, 425206 (2010).